

# Amphiphilic Phospholipid-Based Riboflavin Derivatives for Tumor Targeting Nanomedicines

Nataliia Beztsinna,<sup>†</sup> Yoanna Tsvetkova,<sup>‡</sup> Matthias Bartneck,<sup>§</sup> Twan Lammers,<sup>‡</sup> Fabian Kiessling,<sup>\*,‡</sup> and Isabelle Bestel<sup>\*,†</sup>

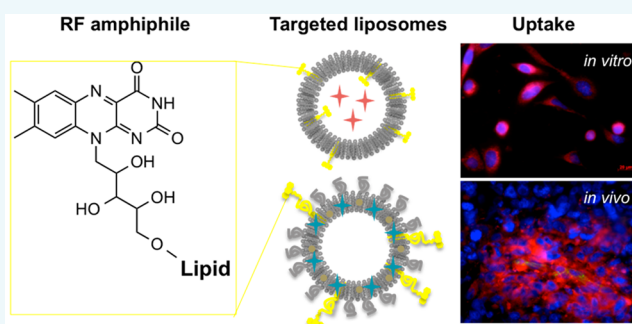
<sup>†</sup>Institute of Chemistry & Biology of Membranes & Nano-objects, CBMN UMR 5248, Bordeaux University, 33600 Pessac, France

<sup>‡</sup>Experimental Molecular Imaging, RWTH Aachen University Clinic, 52056 Aachen, Germany

<sup>§</sup>Gastroenterology and Metabolic Disorders, RWTH Aachen University Clinic, 52056 Aachen, Germany

## S Supporting Information

**ABSTRACT:** Riboflavin (RF) is an essential vitamin for cellular metabolism. Recent studies have shown that RF is internalized through RF transporters, which are highly overexpressed by prostate and breast cancer cells, as well as by angiogenic endothelium. Here, we present an optimized synthesis protocol for preparing tailor-made amphiphilic phospholipid-based RF derivatives using phosphoramidite chemistry. The prepared RF amphiphile—RfdiC14—can be inserted into liposome formulations for targeted drug delivery. The obtained liposomes had a hydrodynamic size of  $115 \pm 5$  nm with narrow size distribution (PDI 0.06) and a zeta potential of  $-52 \pm 3$  mV. In vitro uptake studies showed that RfdiC14-containing liposomes were strongly internalized in HUVEC, PC3, and A431 cells, in a specific and transporter-mediated manner. To assess the RF targeting potential in vivo, an amphiphile containing PEG spacer between RF and a lipid was prepared—DSPE-PEG-RF. The latter was successfully incorporated into long-circulating near-infrared-labeled liposomes ( $141 \pm 1$  nm in diameter, PDI 0.07, zeta potential of  $-33 \pm 1$  mV). The longitudinal  $\mu$ CT/FMT biodistribution studies in PC3 xenograft bearing mice demonstrated similar pharmacokinetics profile of DSPE-PEG-RF-functionalized liposomes compared to control. The subsequent histological evaluation of resected tumors revealed higher degree of tumor retention as well as colocalization of targeted liposomes with endothelial cells emphasizing the targeting potential of RF amphiphiles and their utility for the lipid-containing drug delivery systems.



## INTRODUCTION

Riboflavin (RF) is a water-soluble vitamin (B2) composed from a D-ribitol chain and an isoalloxazine moiety, which is responsible for electronic and optoelectronic properties.<sup>1</sup> Thanks to these features, a number of RF applications in nanotechnology have recently surfaced.<sup>2–8</sup> One could also find RF-based biosensors,<sup>9,10</sup> biocatalysts,<sup>11</sup> and hydrogels,<sup>5,12–14</sup> demonstrating the emerging interest in this molecule in the nanotechnological field.<sup>15</sup>

RF and its derivatives (FMN and FAD) participate in fundamental physiological events in cells including energetic processes, lipid metabolism, and vitamin synthesis. It is not surprising that RF is an essential vitamin for humans. However, it is not synthesized in situ and thus should be obtained from the diet.<sup>1</sup> After ingestion, it is absorbed in the gastro-intestinal tract, distributed within tissues, and taken up by the cells through a specific pathway. The latter involves RF transporters (RFVT-1, RFVT-2, and RFVT-3) and carrier protein (RCP-Riboflavin Carrier Protein).<sup>16–19</sup>

Overexpression of RCP was found in tumor tissues and blood plasma of cancer patients in particular in the case of

breast,<sup>6,7</sup> prostate,<sup>8</sup> and hepatocellular carcinoma.<sup>9</sup> Thus, RF and its derivatives were investigated as a metabolically active cell targeting moiety in dendrimers,<sup>10,11</sup> oligonucleotides,<sup>12</sup> and iron oxide nanoparticles.<sup>13,14</sup> Although these systems showed their targeting efficacy toward cancer cells<sup>2,3,20,21</sup> and neo-vasculature,<sup>7</sup> their acceptance to the clinical practice might be longer compared to conventional widely used lipid-based drug carriers such as liposomes. Another advantage of the liposome-based drug delivery systems is their ability to load both hydrophilic and hydrophobic drugs.<sup>22</sup>

In this study, we developed a versatile chemical strategy for the synthesis of amphiphilic RF derivatives, which could be easily incorporated into lipid-based nanosystems. The established synthetic route delivers RF-phosphoramidite, which is a new building block for design of RF bioinspired phospholipids. Furthermore, due to its fluorescence properties, the amount of RF derivatives in the nanomedicine could be easily quantified. After preparation of RF-functionalized liposomes, their

Received: June 16, 2016

Published: July 14, 2016



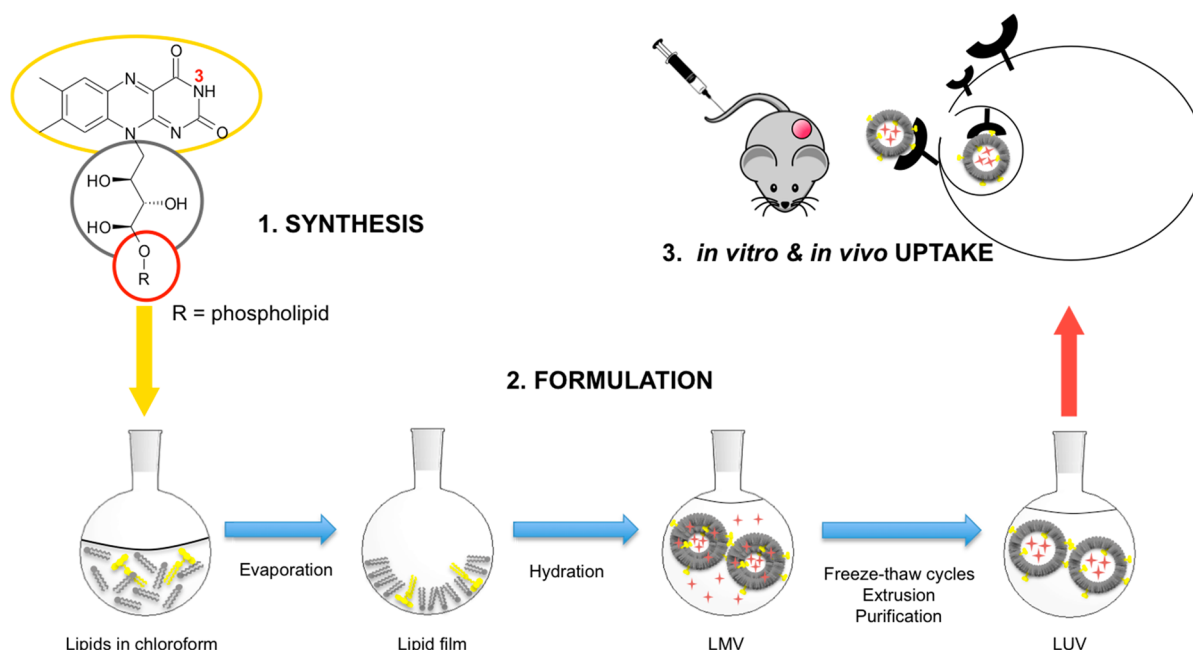
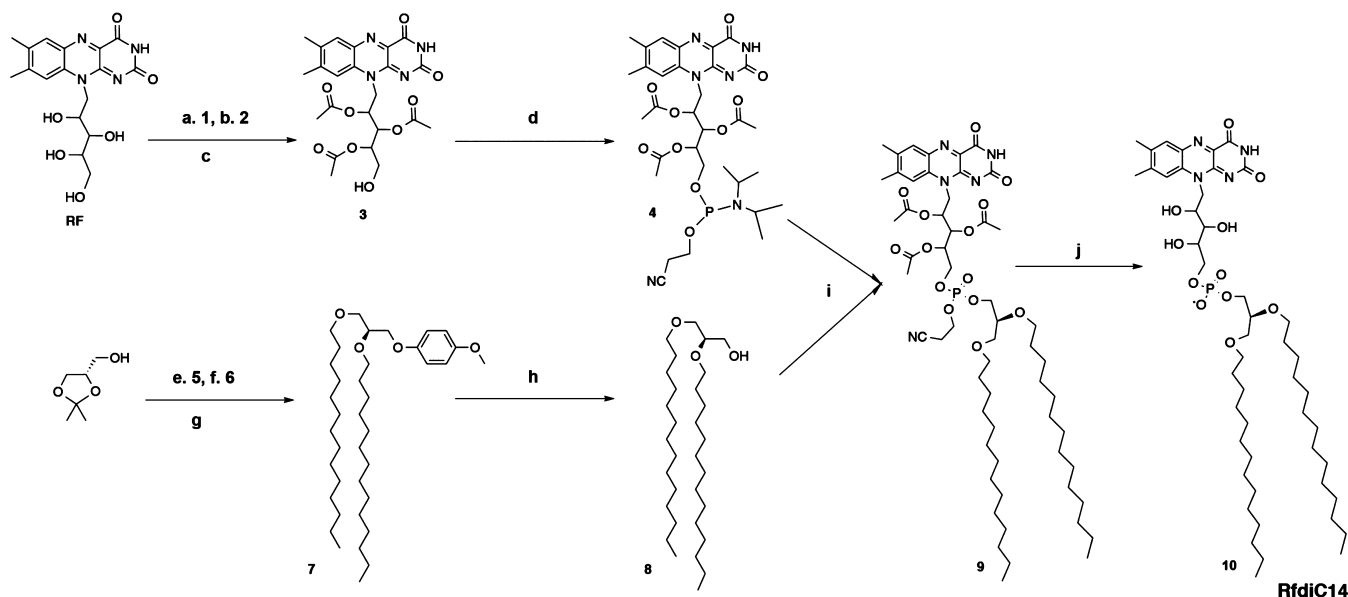


Figure 1. General strategy of the study.

### Scheme 1. RfdiC14 Synthesis<sup>a</sup>

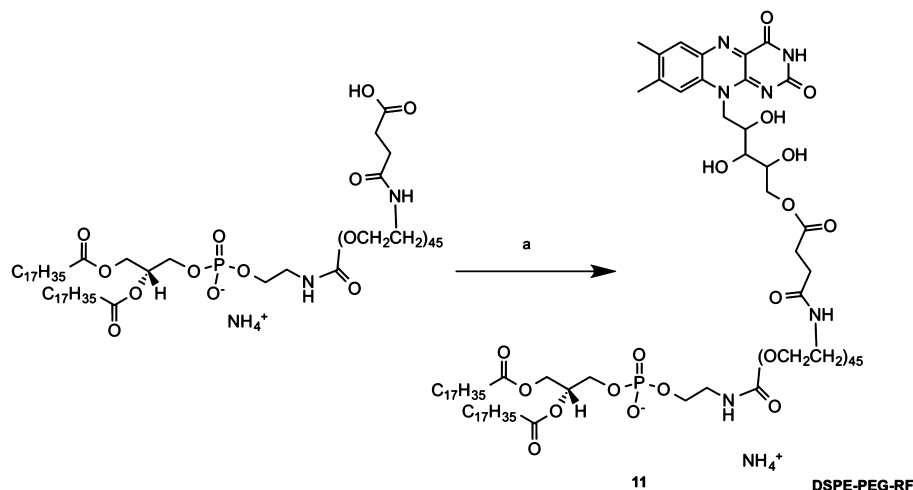


<sup>a</sup>Reagents and Conditions: (a) DMT-Cl, pyridine, TEA, DMAP overnight, rt; (b) Ac<sub>2</sub>O, pyridine, overnight, rt; (c) ZnBr<sub>2</sub>, nitromethane, 10 min, rt; (d) 2-cyanoethyl-*N,N*-diisopropylchlorophosphoramidite, DIPEA, DCM, overnight, rt; (e) PMP, triphenylphosphine, DEAD, 3 h, rt; (f) DOWEX 50 H<sup>+</sup>, MeOH, overnight, rt; (g) NaH, C14-Br, DMF, overnight, rt; (h) ceric ammonium nitrate, acetonitrile/H<sub>2</sub>O (8:2), overnight, rt; (i) 5-benzylthio-1*H*-tetrazole, THF, 6 h, rt, then 0.2 M iodine in THF/pyridine/H<sub>2</sub>O (2:1:1), overnight, rt; (j) MeONa/MeOH, 24 h, rt.

physicochemical characterization was performed and their specific cell internalization demonstrated in cancer cells A431 (human epidermal cervix carcinoma), PC3 (prostate cancer), and human umbilical vein endothelial cells (HUVEC) that mimic activated tumor neovasculature. Moreover, for the subsequent in vivo studies a RF amphiphile bearing a polyethylene glycol (PEG) spacer between RF and a lipid was prepared. The biodistribution and tumor accumulation of RF-amphiphile functionalized long-circulating liposomes was studied in nude mice bearing PC3 tumor xenografts. The general strategy of the study is described in Figure 1.

## RESULTS AND DISCUSSION

**Chemistry and Molecule Design.** In order to prepare an amphiphilic derivative, one has to adjust a certain hydrophobic/hydrophilic balance in the molecule. Although RF belongs to the family of water-soluble vitamins, it displays a rather poor solubility in water (1 g in 10 L). Moreover, its solubility in organic solvents is also complex. Due to its poor solubility in both water and organic solvents, the chemical modification of RF represents a real challenge. This behavior could be related to inherent amphiphile properties of the molecule—the isoalloxazine ring responsible for hydrophobicity and the ribitol

Scheme 2. DSPE-PEG-RF Synthesis<sup>a</sup>

<sup>a</sup>Reagents and conditions: (a) RF, DMF, DCC, DMAP 48 h, rt.

chain responsible for hydrophilicity. Nevertheless, the molecule by itself does not form any autoassemblies. In our strategy, we tuned both the hydrophilic and hydrophobic properties of RF. For this purpose we attached lipid chains through a charged phosphodiester chemical group leading to a bioinspired phospholipid derivative.

Based on the chicken RCP crystallization data,<sup>23</sup> two sites of the molecule appear suitable for the modification: the N3 position and the primary alcohol of the ribitol chain. In fact, RF binds into a folded pocket of the RCP involving stacking interactions between the isoalloxazine moiety and the aromatic rings of Tyr75 and Trp156 residues. This gives the possibility to modify N3 or primary alcohol group of RF without significant impact on its binding affinity toward the RCP.

With the aim of mimicking natural phospholipids as well as the biological derivative of RF—FMN (flavin mononucleotide), we mainly focused on the ribitol chain substitution by using a phosphate linker. Although a previous study showed a small decrease in the affinity of RF derivatives bearing a ribitol linkage compared to N3 substitution,<sup>24</sup> it nevertheless ensured cancer cell targeting.<sup>25</sup>

The versatile synthesis route for the preparation of RF-based phospholipid is depicted in Scheme 1. This is a convergent approach based on a phosphoramidite coupling between the functionalized RF derivative 4 and the glycerolipid moiety 8. The former was obtained in four steps: orthogonal protections of hydroxyl groups—DMT for the primary alcohol (1), acetate protection for the secondary alcohols (2),<sup>26</sup> then selective cleavage of DMT by zinc bromide (3), and finally treatment with phosphorylating agent (4). The generated RF-phosphoramidite 4 was further coupled with a glycerolipid bisubstituted with C14 chains (8). The latter was classically prepared in four steps (5–8) from solketal (Supporting Information, Figures S5–6 and S8).

After coupling 4 and 8, a final cleavage of all protecting groups was performed to afford RfdiC14 (10), which was further characterized by <sup>1</sup>H, <sup>13</sup>C, and <sup>31</sup>P NMR, and ESI-MS (Supporting Information, Figures S1–4 and S9).

This chemical strategy allows the coupling of different lipids to the phosphoramidite intermediate 4 and is as an adaptable approach to generate a library of amphiphilic RF derivatives with various lipid moieties.

For further in vivo evaluation of RF targeting potential, we prepared an analogous derivative of RfdiC14 including a PEG spacer. The molecule contains a PEGylated lipid coupled to RF moiety at the 5' O position. A commercially available phospholipid that holds an NHS-activated carboxylic acid at the terminal of a PEG spacer—DSPE-mPEG2000-succinyl (1,2-distearoyl-*sn*-glycero-3-phosphoethanolamine-*N*-[succinyl (polyethylene glycol)-2000])—was coupled to a nonprotected RF via a Steglich esterification.<sup>27</sup> The use of previously developed RF-phosphoramidite was not possible for this derivative due to the presence of glycerol esters in the DSPE-mPEG2000, which could be cleaved during the final deprotection step.

The PEGylated RF amphiphile was prepared in one step as depicted on Scheme 2 and named DSPE-PEG-RF (11). TLC and reverse-phase HPLC analysis confirmed the formation of a new product, which was purified with reverse-phase HPLC and analyzed with MALDI-MS (matrix-assisted laser desorption ionization mass spectrometry) (Supporting Information Figure S10). The purification from the lipid-PEG precursor was not complete, but its presence did not cause any negative effect on subsequent liposome formation since the DSPE-PEG is classically used in the formulation to ensure long-circulating properties. This newly synthesized PEGylated RF amphiphile was further used for the preparation of long-circulating targeted liposomes.

**Formulation. Bare Liposomes.** Due to its double myristyl chain, RfdiC14 can be inserted into almost any lipid formulation such as micelles, liposomes, nanoemulsions, and lipid nanoparticles.

The selected model liposome formulation (DMPC:DMPG) is clinically used as a drug delivery system, available on the market as Abelcet (encapsulated Amphotericin B).<sup>22</sup> Since RfdiC14 has similar lipid chain length as DMPC and DMPG, it could be easily incorporated into the liposome bilayer. We obtained stable liposomes with molar ratio of 90:10:1 for DMPC:DMPG:RfdiC14 by film hydration method followed by extrusion through 100 nm polycarbonate membrane and gel filtration on a G25 Sephadex column. To ensure the proper incorporation of RfdiC14 into the liposome membrane, RfdiC14 was dissolved in chloroform and mixed with DMPC and DMPG during the lipid film preparation. A post-insertion

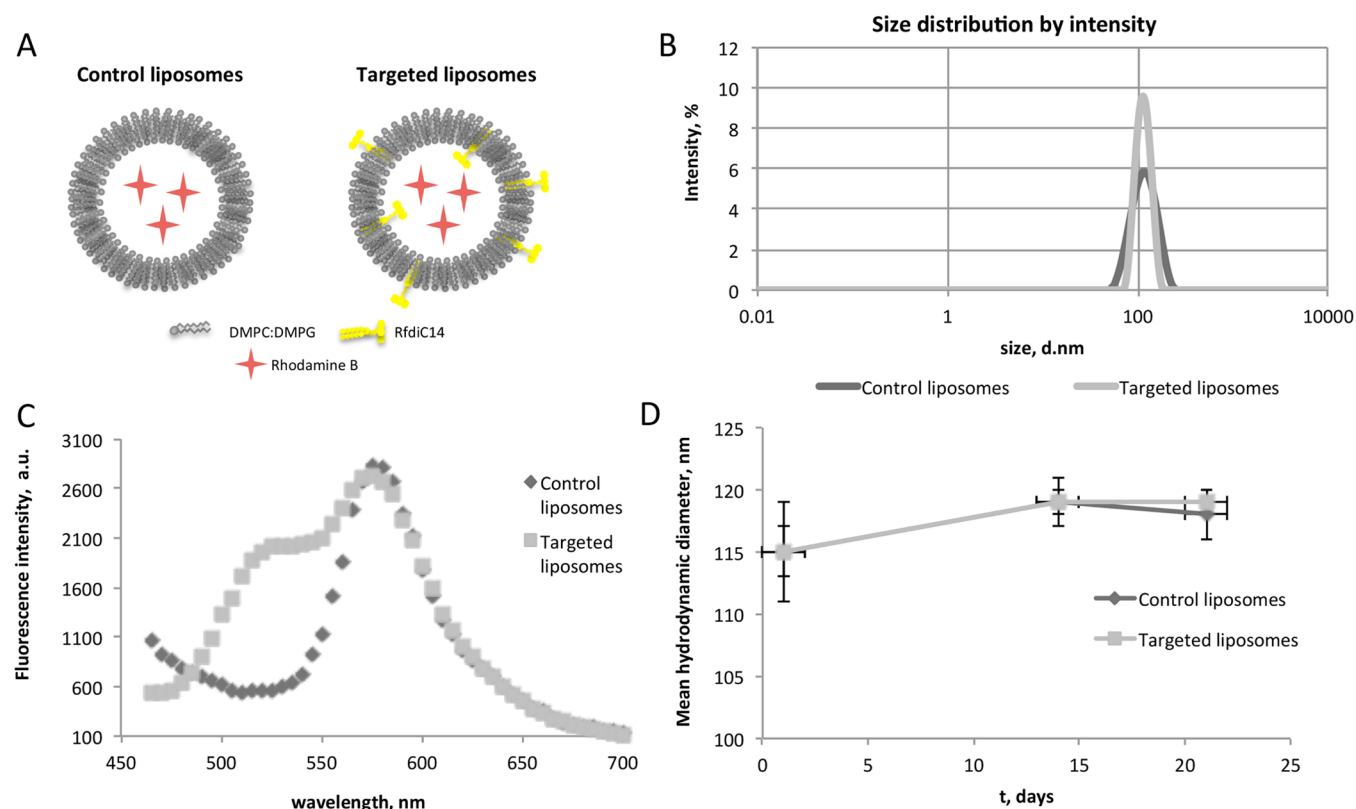


**Figure 2.** A. Schematic representation of bare liposomes. B. Hydrodynamic size and size distribution of control (dark gray) and RfdiC14-tagged (light gray) liposomes. C. Fluorescence emission spectra of control and targeted liposomes. D. Size stability of liposomes during storage.

**Table 1. Physicochemical Properties of Prepared Formulations**

formulation	hydrodynamic diameter, nm	polydispersity index	zeta potential, mV	dye, $\mu\text{M}$
Control liposomes DMPC:DMPG 90:10	$115 \pm 5$	0.10	$-52 \pm 2$	5.7
Targeted liposomes DMPC:DMPG:RfdiC14 90:10:1	$115 \pm 2$	0.06	$-51 \pm 3$	5.1
Control long-circulating liposomes DPPC:Chol:DSPE-PEG:DiR 65:30:5:0.5	$137 \pm 2$	0.06	$-18 \pm 1$	38
Targeted long-circulating liposomes DPPC:Chol:DSPE-PEG-RF:DiR 65:30:5:0.5	$141 \pm 1$	0.07	$-33 \pm 1$	37

of RfdiC14 in already formed liposomes was not as efficient because of RfdiC14 auto-organization and aggregation in buffer.

Rhodamine B (RhB) was encapsulated as a model drug in the aqueous phase of the liposomes (Figure 2A), which allowed the evaluation of cellular uptake by fluorescence microscopy ( $\lambda_{\text{ex}}$  554 nm). The presence of RhB and RfdiC14 in the formulated liposomes was confirmed and quantified spectroscopically (Figure 2C). As control liposomes contain only RhB, they exhibit single emission peak at 580 nm, whereas targeted liposomes display two emission maxima—580 nm for RhB and 530 nm for RfdiC14. The exact amount of each fluorophore in the formulation was calculated with the help of calibration curves— $y = 5987x$  ( $R^2 = 0.9939$ ) for RF and  $y = 17888x$  ( $R^2 = 0.98918$ ) for RhB, where  $y$  represents the fluorescence intensity and  $x$  the concentration in  $\mu\text{M}$  (Supporting Information, Figure S11). The insertion efficiency of RfdiC14 was always close to 100% with respect to the starting composition (0.2  $\mu\text{mol}$  of RF for 20  $\mu\text{mol}$  of total lipid content represents the desired 1% molar). This signifies that RfdiC14 was efficiently entrapped in the lipid bilayer. Direct quantification of RfdiC14 in liposomes by fluorescence represents an advantage of this targeting moiety compared to other commonly used targeting ligands such as

antibodies or peptides that require more sophisticated quantification methods (e.g., ELISA, HPLC).

The physicochemical properties of the RF-functionalized liposomes (targeted) in terms of hydrodynamic diameter, core size, polydispersity, and zeta potential were compared to RfdiC14-free liposomes (control) (Table 1). Both control and targeted liposomes had similar hydrodynamic size of  $115 \pm 5$  nm (PDI < 0.1, Figure 2B) and negative zeta potential of  $-52 \pm 3$  mV. Such negative zeta potential could be due to the presence of negatively charged DMPG lipid. For this reason, liposomes exhibited good colloidal stability in buffer during at least 3 weeks storage at 4 °C. Thus, the hydrodynamic size measurements (Figure 2D) did not show significant differences over time. The cryo-EM analysis of targeted liposomes revealed unilamellar vesicles with a mean diameter of  $88 \pm 16$  nm (Supporting Information, Figure S13.A). In order to assess the possible changes that RfdiC14 could induce in the DMPC:DMPG membrane, we performed a deuterium solid-state NMR (ssNMR) experiment (Supporting Information, Figure S13.B) and studied the potential RhB leakage after 2 weeks of storage at 4 °C or 30 min incubation at 37 °C (Supporting Information, Figure S13.C). ssNMR spectra (in the range of tested temperatures) as well as the calculation of



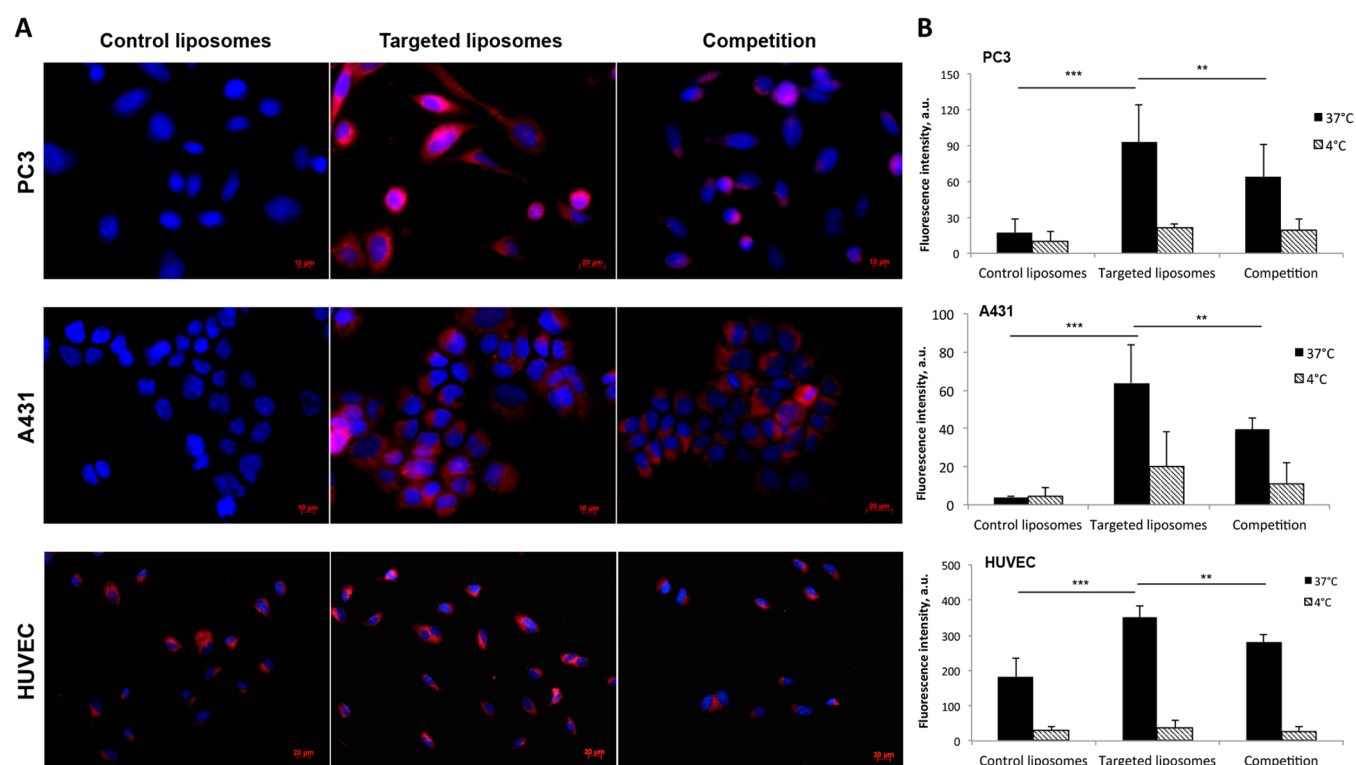


**Figure 3.** Cellular uptake of control and targeted liposomes: A. Fluorescence microscopy images of uptake in different cell lines. Nuclei are marked in blue with DAPI, RhB-containing liposomes are depicted in red. B. Uptake quantification by measuring fluorescence intensity,  $\lambda_{\text{ex}}$  554 nm,  $\lambda_{\text{em}}$  605 nm. Results presented as average  $\pm$  SD of 3 individual experiments, for each experiment from 10 to 20 images per condition were evaluated (\*\* $p < 0.001$ , \*\* $p < 0.01$ ), SD = standard deviation.

order parameters revealed no significant differences in membrane organization in the presence or absence of RfdiC14. This agrees with the absence of RhB leakage observed during stability studies.

The above-mentioned results indicate that the presence of RfdiC14 does not perturb the DMPC:DMPG membrane. RhB-free targeted liposomes were prepared for competitive binding experiments.

**Long Circulating Liposomes.** As a long-circulating formulation, we chose the extensively studied DPPC:Cholesterol:DSPE-PEG2000 lipid composition in 65:30:5 molar ratios<sup>22,28,29</sup> (Figure 5A). In targeted formulation DSPE-PEG2000 was replaced by a mixture of DSPE-PEG-RF and DSPE-PEG-COO<sup>-</sup>. The preparation method was the same as that for the above-mentioned bare liposomes. Control long-circulating liposomes (LCL) had a mean hydrodynamic diameter of  $137 \pm 2$  nm (PDI 0.06) and a negative zeta potential of  $-18 \pm 1$  mV. Targeted LCL had slightly greater size of  $141 \pm 1$  nm (PDI 0.07) and a more important zeta potential of  $-33 \pm 1$  mV. The more negative zeta potential of targeted LCL could be explained by the presence of unconjugated DSPE-PEG-COO<sup>-</sup>, which could not be separated from RF amphiphile.

A near-infrared lipophilic dye—DiR (1,1'-dioctadecyl-3,3,3',3'-tetramethylindotricarbocyanine iodide)—was encapsulated to track liposome biodistribution in vivo.<sup>30</sup> Due to its hydrophobic character, DiR was dissolved in chloroform and added to the initial lipid mixture (0.5% molar ratio) during the lipid film preparation step. Similarly to previously described bare liposomes, the presence of RF amphiphile and DiR in the liposomes was confirmed and quantified spectroscopically. In the fluorescence emission spectra one can observe a character-

istic emission of RF at 530 nm for targeted liposomes and the DiR emission peak at 782 nm for both formulations. The calibration curve was used to assess the dye concentration in liposomes  $y = 7200x$  ( $R^2 = 0.9916$ ), where  $y$  represents DiR fluorescence intensity and  $x$  the concentration in  $\mu\text{M}$  (Table 1). According to the RF fluorescence intensity measurements the actual amount of RF in targeted LCL was around 0.35% molar (Figure 6B; for RF calibration curve see Supporting Information, Figure S11). Both targeted and control LCL exhibited decent size stability during storage (no significant size and PDI increase after 2 weeks of storage at 4 °C, data not shown).

Additionally, for the in vivo imaging studies, the fluorescence signal intensity generated by targeted LCL was evaluated in specifically designed polymeric phantom by combined  $\mu\text{CT}$ /FMT imaging.<sup>31</sup> The 3D reconstruction of the phantom volume based on  $\mu\text{CT}$  images yielded fluorescence intensity values for each LCL concentration tested. The obtained values were plotted against DiR quantity in nmol (Supporting Information, Figure S12) and used for the quantification of LCL accumulation in vivo.

**In Vitro Evaluation. Bare Liposomes.** The targeting efficiency of RfdiC14 liposomes was evaluated by fluorescence microscopy for the cancer cell lines A431 and PC3, and in human umbilical vein endothelial cells (HUVEC), the latter used as a model of activated tumor neovasculature (Figure 3). The highest uptake of targeted liposomes was found for A431 cells ( $62 \pm 23$  au), 16 times higher compared to control liposomes ( $4 \pm 1$  au),  $p < 0.001$ . In the case of PC3 cells, the uptake of targeted liposomes was 5 times higher than the above-mentioned control liposomes  $90 \pm 31$  vs  $17 \pm 11$  au ( $p < 0.001$ ). Compared to the cancer cell lines, HUVECs showed

## PC3

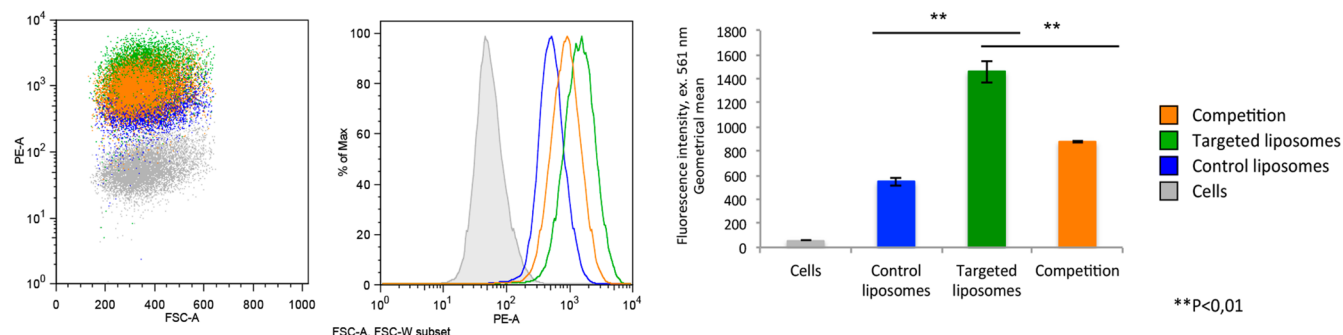


**Figure 4.** Flow cytometric analysis of liposome uptake by PC3 cells ( $\lambda_{\text{ex}}$  561 nm); the values are presented as geometrical mean  $\pm$  SD from  $n = 3$  experiments. (\*\* $p < 0.001$ , \* $p < 0.01$ ).

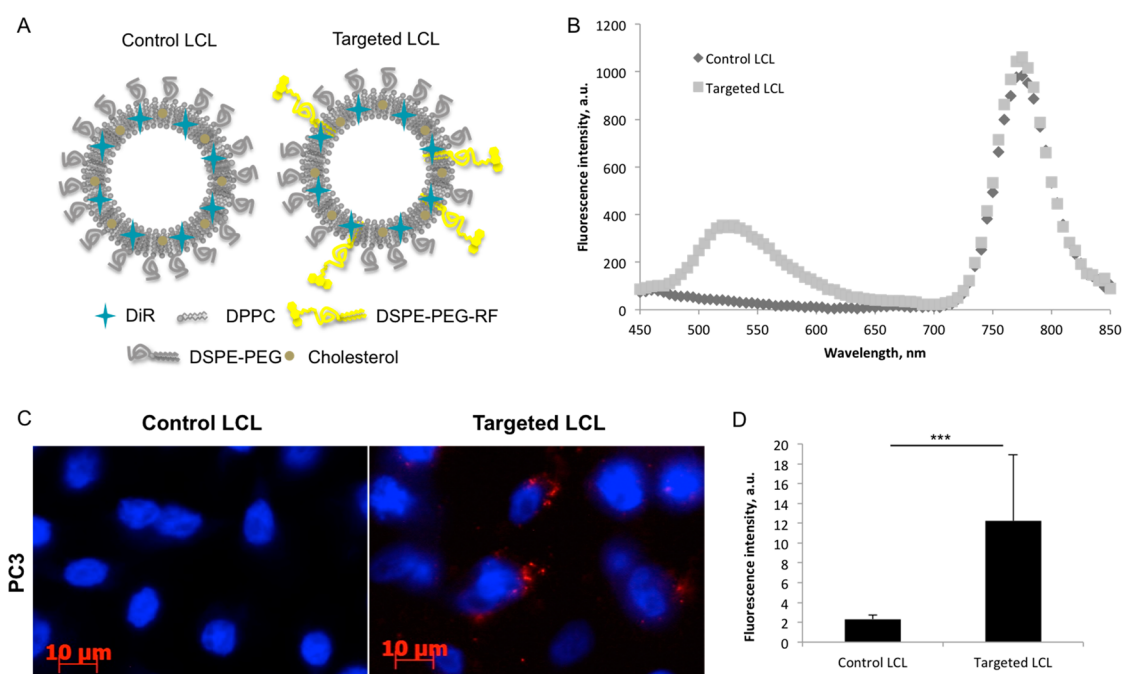


**Figure 5.** A. Schematic representation of LCL. B. Fluorescence emission spectra of control and targeted LCL. C. Fluorescence microscopy images of LCL uptake in PC3 cell line. Nuclei are marked in blue with DAPI, DiR-containing liposomes are depicted in red. D. Uptake quantification by measuring fluorescence intensity,  $\lambda_{\text{ex}}$  750 nm,  $\lambda_{\text{em}}$  780 nm. Results presented as average  $\pm$  SD of 3 individual experiments, for each experiment from 10 to 20 images per condition were evaluated (\*\* $p < 0.001$ ), SD = standard deviation.

higher liposome internalization for both targeted and control formulations. However, the uptake of RfdiC14 liposomes was still twice as high as that for the nontargeted liposomes ( $358 \pm 20$  compared to  $149 \pm 12$  au ( $p < 0.001$ )).

Although the cellular uptake of RF-liposomes varies among the studied cell lines the results clearly show that RfdiC14 increases liposome uptake. According to the database of the Human Protein Atlas (<http://www.proteinatlas.org/>), RNA expression of RFVT-2 (SLC52A2) transporter is ubiquitous in all reported cancer cell lines, though the amount varies among them. The PC3 cell line exhibited the highest level of RFVT-2 RNA expression compared to others. In spite of the lower level of RFVT-2 RNA expression, the A431 cell line displayed higher targeted versus control uptake ratio in our studies. However, the nonspecific membrane binding of targeted liposomes at low temperature was also greater for these cells (Figure 3).

In addition, competitive binding experiments proved that the presence of RF is essential for cellular uptake and confirmed the

specificity of RfdiC14-tagged liposomes toward RF transporters. The uptake of targeted liposomes significantly decreased ( $p < 0.01$ ) by 31% for PC3, 37% for A431, and 20% for HUVEC under competition with 20-fold excess of RfdiC14-tagged nonfluorescent liposomes. These data are in agreement with our previous studies<sup>2</sup> indicating a decrease by 15–30% in the internalization of RF-functionalized ultrasmall ferrum oxide nanoparticles (FLUSPIOs) when the cells were preincubated with an excess of RF derivative. Furthermore, a significant decrease ( $p < 0.01$ ) in the uptake of targeted liposomes at 4 °C was observed for all cell lines (Figure 3). Thus, we hypothesize that the RfdiC14-tagged liposomes were internalized in a specific manner.

Additionally, flow cytometric analysis of liposome uptake by PC3 cells ( $\lambda_{\text{ex}}$  561 nm;  $\lambda_{\text{em}}$  578 nm) confirmed the obtained results from fluorescence microscopy evaluation (Figure 4). This complementary approach allows simultaneous analysis of a high number of cells. The targeted liposome uptake was 28

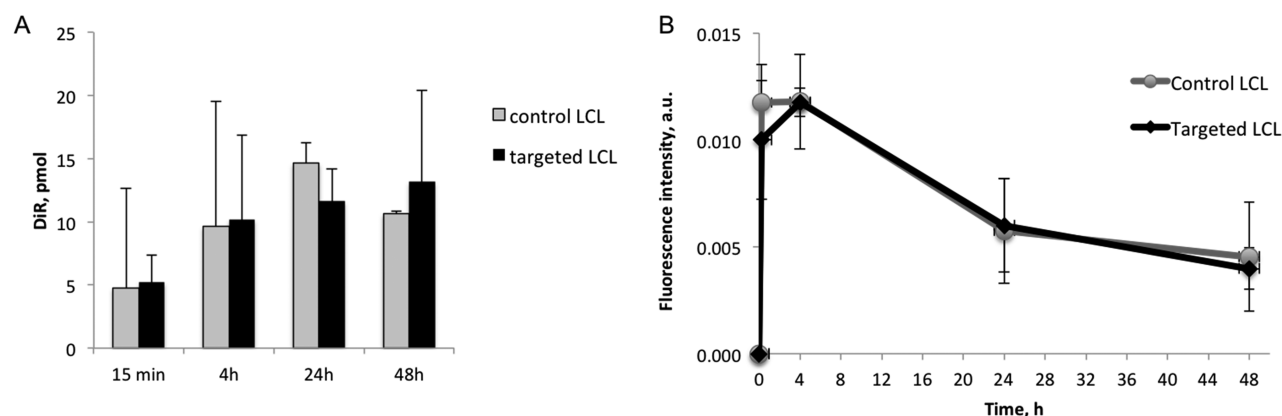


**Figure 6.** A. Longitudinal fluorescence quantification in PC3 tumor xenografts after i.v. injection of control or targeted LCL. B. Pharmacokinetics of control and targeted LCL measured with 2D FRI from blood spots. Results presented as average  $\pm$  SD from  $n = 3$  mice per group, SD = standard deviation.

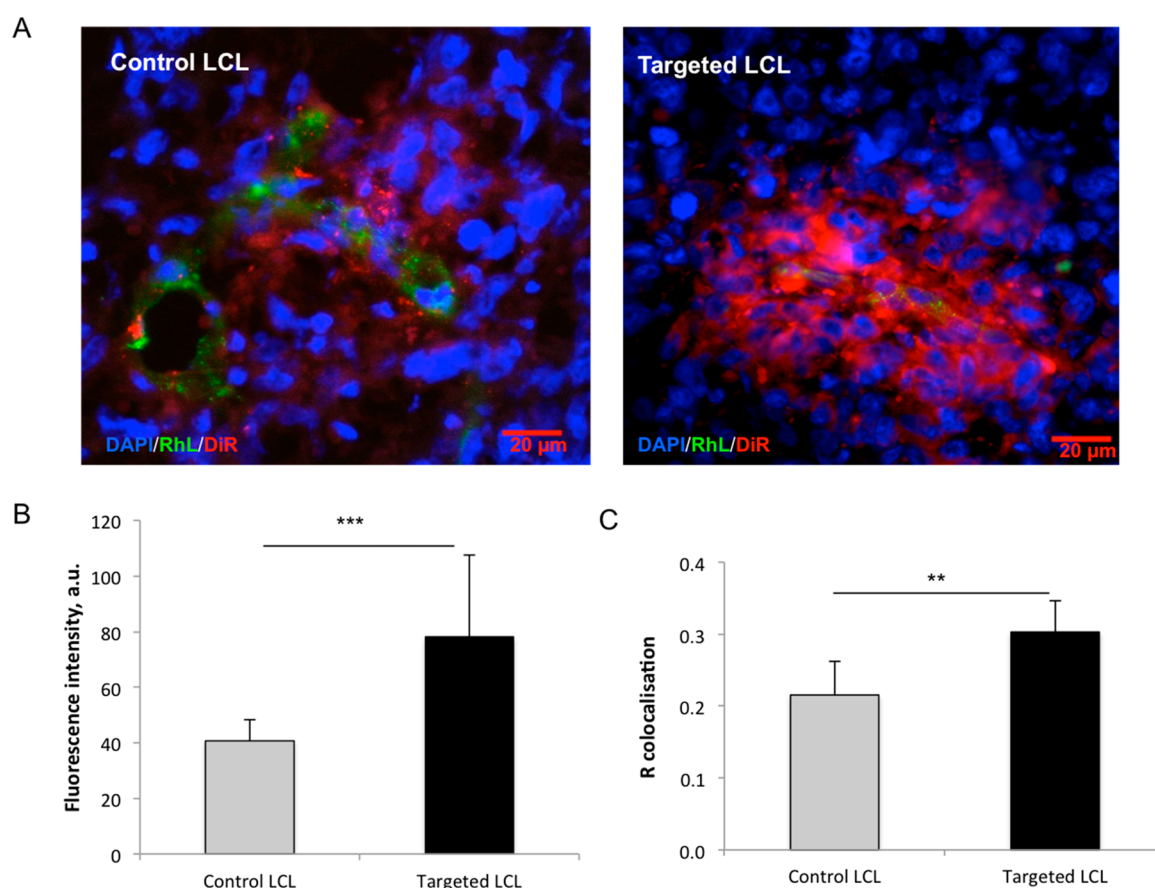


**Figure 7.** A. Fluorescence microscopy images from tumor cryosections; nuclei are stained in blue with DAPI, endothelial cells in green with Rhodamine-Lectin and targeted or control LCL are presented in red. B. Quantification of control and targeted LCL signal in fluorescence microscopy images from tumor cryosections. C. Quantification of colocalization between endothelial cells and LCL. Results are presented as mean from  $n = 3$  tumors per group and 15–25 images for each tumor  $\pm$  SD (\*\*\* $p < 0.001$ , \*\* $p < 0.01$ ), SD = standard deviation.

times higher than basic cell fluorescence level and 2.7 times higher than ( $p < 0.01$ ) the uptake of control liposomes. In accordance with the fluorescence microscopy study, a competitive binding experiment revealed a 40% decrease in targeted liposomes accumulation.

Finally, a standard MTT cell viability test for the evaluation of RfdiC14 liposomes cytotoxicity was performed. For this purpose, the cells were incubated either with 3 concentrations of control/targeted liposomes: 50 nM – 1x, 150 nM – 3x, and

250 nM – 5x for 72 h or with buffer (Control). The relative viability was expressed in % and calculated by the ratio between formed formazan crystal absorbance of treated and untreated cells (Supporting Information, Figure S14). The study revealed no specific cytotoxicity associated with RfdiC14-tagged liposomes compared to controls. The 40–60% decrease in viability at 3x and 5x concentration is most probably associated with general toxicity of RhB administrated in high doses.<sup>32</sup>



**Long-Circulating Liposomes.** Prior to the *in vivo* assessment, we verified that this new formulation (DSPE-PEG-RF) conserved targeting abilities. The *in vitro* uptake of LCL targeted liposomes was investigated in PC3 cell line (Figure 5C,D). The quantification of DiR fluorescence in PC3 cells revealed 6 times significantly higher signal from targeted LCL ( $12.2 \pm 6.7$  au) compared to control ( $2.3 \pm 0.4$  au;  $p < 0.001$ ). These results are very similar to those observed with RfdiC14 functionalized liposomes confirming that the PEGylation of liposome surface and the spacer between RF and lipid did not influence RF targeting potential.

**In Vivo Evaluation.** Due to the presence of several transporter systems (SLC52 family and RCP) the evaluation of RF-targeting *in vivo* might be a complex issue. Moreover, targeted nanoparticles are often known to perform worse than nontargeted *in vivo* due to accelerated clearance and/or limited tumor penetration as a result of opsonization triggered by the presence of targeting moiety.<sup>33–35</sup> Thus, in this pilot study we aimed to compare the pharmacokinetics and biodistribution of targeted LCL with control LCL and assess their potential in targeting tumor and neovasculture.

The study was performed in nude mice bearing PC3 tumor xenografts. The animals ( $n = 6$ ) were divided into two groups and each received a single *i.v.* injection of either targeted or control LCL. The whole body  $\mu$ CT (micro computed tomography) and FMT (fluorescence mediated tomography, ex. 750 nm, em. 780 nm) scans were performed at defined time points after injection. The  $\mu$ CT/FMT data fusion, reconstruction, and 3D quantification<sup>36</sup> of liposome biodistribution in healthy organs showed similar results for both targeted and control LCL (Supporting Information, Figure S16.A). The highest accumulation was observed in the liver for all time points and in the heart 15 min after injection. The 2D fluorescence reflectance imaging (FRI) of excised organs confirmed these results (Supporting Information, Figure S16.B). The majority of fluorescence signal was detected in the liver and spleen. Although compared to conventional liposomes the PEGylation limits opsonization and macrophage uptake,<sup>29</sup> these organs are still responsible for liposome excretion.<sup>37</sup>

The 2D FRI of fluorescence signal assessment in blood revealed similar pharmacokinetics profiles for both formulations with a half-life of 24 h (Figure 6.B). This signified that the presence of RF amphiphile in the liposome formulation did not accelerate the blood clearance and liposomes keep their long-circulating properties. The tumor accumulation evaluation in 3D over time did not show significant differences between control and targeted LCL (Figure 6A), whereas the histological analysis of excised tumor cryosections demonstrated significantly higher ( $p < 0.001$ ) fluorescence signal in animals that received targeted LCL ( $78.2 \pm 29.4$  au) compared to nontargeted ( $40.8 \pm 7.6$  au). This might be explained by the partial elimination of control liposomes from the cryosections during several washing steps that are necessary for preparation, while targeted liposomes were most likely retained due to their affinity to RF transporters and putative cellular internalization. A similar phenomenon was observed by Kirpotin et al.<sup>38</sup> with long-circulating immunoliposomes. Moreover, the colocalization analysis revealed a more important association ( $p < 0.01$ , Figure 7A,C) of targeted LCL with the endothelial cells of tumor neovasculture (labeled with Rhodamine-Lectin). These data are in accordance with the predominant vascular

localization of RF-functionalized ferrum oxide nanoparticles (FLUSPIOs) *in vivo*.<sup>7,39</sup>

Taken together, the presence of RF amphiphile in the liposome formulation mediates enhanced uptake *in vitro* and does not alter the pharmacokinetics of liposomes *in vivo*. Even though the 3D quantification *in vivo* did not reveal differences in the overall tumor accumulation, the increased retention in the tumor and colocalization with endothelial cells were observed for targeted LCL. While the functional EPR effect is the major driving force for the LCL tumor accumulation,<sup>33,34</sup> the liposome functionalization with an RF amphiphile might increase tumor retention and mediate subsequent uptake in endothelial and cancer cells. Thus, in agreement with our studies and the literature,<sup>3,7,39,40</sup> RF-based targeting is a promising approach for prostate, breast, hepatocellular, and epidermoid carcinomas as well as tumor neovasculture. On the other hand, because the exact targeting route of RF-conjugated nanoparticles and macromolecules is still poorly understood, our RF amphiphiles could be also used as functional tools for the investigation of RF targeting and internalization pathways *in vitro* and *in vivo*.

## CONCLUSIONS

In summary, this study describes the synthesis of two amphiphilic derivatives of RF through the phosphoramidite and esterification approaches. The key intermediate of the former, RF-phosphoramidite, can be used as a building block for tailor-made RF derivatives. The prepared amphiphile, RfdiC14, is a bioinspired phospholipid that was inserted into a clinically relevant liposome formulation without influence on liposome stability, morphology, and toxicity. Cell uptake studies using PC3 and A431 cells and HUVECs showed efficient and competitive internalization of RfdiC14 liposomes. A PEGylated RF amphiphile, DSPE-PEG-RF, suitable for *in vivo* applications was also prepared. Similarly to the RfdiC14, it demonstrated successful insertion into long-circulating NIR-labeled liposomes and the enhanced uptake of these liposomes in the PC3 cell line. The  $\mu$ CT/FMT imaging studies in PC3 tumor-bearing mice showed that the presence of DSPE-PEG-RF does not compromise liposome pharmacokinetics or significantly alter organ distribution when compared to the nontargeted formulation. Moreover, histological analysis of resected tumors indicated higher retention and endothelial cell targeting potential of RF-tagged liposomes. Therefore, RF amphiphiles are considered to be a useful tool for functionalizing amphiphilic drug delivery systems, such as liposomes. This approach could be extended to micelles, lipidic nanoparticles, or nanoemulsions. When such systems are used as cytostatic drug carriers, an insertion of an RF amphiphile could enable targeted drug delivery to tumors by addressing its vascular and tumor cell compartment.

## EXPERIMENTAL SECTION

**Chemicals and Analytical Conditions.** All reagents and solvents were purchased from Sigma-Aldrich, Bachem, Glen Research, and Alfa Aesar and were utilized without further purification. All synthesized compounds were characterized using  $^1\text{H}$ ,  $^{13}\text{C}$ , and  $^{31}\text{P}$  NMR spectroscopy (apparatus Bruker Avance DPX-300,  $^1\text{H}$  at 300 MHz,  $^{13}\text{C}$  at 75 MHz, and  $^{31}\text{P}$  at 121 MHz or Bruker Avance DPX-400,  $^1\text{H}$  at 400 MHz,  $^{13}\text{C}$  at 100 MHz, and  $^{31}\text{P}$  at 162 MHz) and mass spectrometry. The NMR chemical shifts are reported in parts per million relative



to the tetramethylsilane, using the deuterium signal of the solvent ( $\text{CDCl}_3$ , MeOD, or deuterated dimethyl sulfoxide  $\text{DMSO}-d_6$ ) as a heteronuclear reference for  $^1\text{H}$ . 1D spectra were acquired by mean of a classical  $90^\circ$  pulse sequences for the  $^1\text{H}$ ,  $90^\circ$  pulse sequences with an inverse-gated decoupling during the acquisition for the  $^{31}\text{P}$  and  $90^\circ$  pulse sequences with a power-gated decoupling for the  $^{13}\text{C}$ . 2D spectrum was acquired by mean of a HMQC sequence ( $^1\text{H}/^{13}\text{C}$  correlation via heteronuclear multiquantum coherence). The  $^1\text{H}$  NMR coupling constants,  $J$ 's, are reported in Hz.

Electrospray ionization mass spectra (Full ESI-MS) were obtained by the "Mass Spectrometry Platform" in IECB (Bordeaux, France) on Agilent 6560 ESI-IMS-Q-TOF apparatus. For the PEGylated sample an Ultraflex III MALDI-TOF-TOF instrument (Bruker Daltonics GmbH, Bremen, Germany) equipped with a Smartbeam 2 laser with a repetition rate up to 200 Hz (500 laser shots) was used. The obtained mass spectrum was analyzed with Flex-analysis v 4.0 software (Bruker Daltonics GmbH, Bremen, Germany).

For the flash chromatography, silica gel 60 (particle size: 45  $\mu\text{m}$ , Biotage) was utilized. Aluminum plates coated with silica gel 60 F254 (Merck) were used for thin layer chromatography (TLC). The TLC plates were analyzed with visible/UV light or revealed with phosphomolybdic acid solution (10%). HPLC and GPC separation and analysis were performed with Waters Alliance 2695 (Waters Corporation, USA) apparatus equipped with the UV-detector Waters 486 and Waters 2475 FLR detector (Waters Corporation, USA) and analyzed with Millennium 32 software (Waters Corporation, USA). The reverse phase analytical C8 column (Macherey-Nagel, GmbH&Co, KG) was used for all HPLC separations. The BioSep-SEC-S3000 (Phenomenex, Torrance, USA) was used for GPC separations.

Cell culture media and additives were from Gibco/Life Technologies, Carlsbad, California.

**Synthesis.** 10-(5-(Bis(4-methoxyphenyl) (phenyl)-methoxy)-2,3,4-trihydroxypentyl)-7,8-dimethylbenzo[g]pteridine-2,4(3H,10H)-dione (Compound 1). This was synthesized as described previously.<sup>26</sup> Briefly, riboflavin (807 mg, 2.14 mmol) was dissolved in dry pyridine (100 mL) under argon atmosphere. Then TEA (3.6 equiv, 1 mL, 7.7 mmol), DMAP (0.05 equiv, 13 mg, 0.1 mmol), and 4,4'-dimethoxytrityl chloride (1.3 equiv, 915 mg, 2.7 mmol) were added. The reaction mixture was stirred overnight at rt. To stop the reaction 15 mL of methanol were added and organic solvents were evaporated under reduced pressure. The crude product was dissolved in DCM, then filtered, evaporated, and purified by silica gel column chromatography (DCM/MeOH/TEA 97/2/1) to afford an orange solid. Yield: 510 mg (0.75 mmol, 35%).

$^1\text{H}$  NMR (300 MHz,  $\text{DMSO}-d_6$ ):  $\delta$  (ppm) = 2.39 (s, 3H,  $\text{CH}_3$ ), 2.41 (s, 3H,  $\text{CH}_3$ ), 3.05–3.18 (m, 2H,  $\text{CH}_2\text{-O}$ ), 3.72 (s, 6H,  $2 \times \text{CH}_3\text{-O}$ , DMT), 3.92 (s, 1H,  $\text{CH-O}$ ), 4.23 (s, 1H,  $\text{CH-O}$ ), 4.63 (m, 1H,  $\text{CH}_2\text{-N}$ ), 4.94 (m, 1H,  $\text{CH}_2\text{-N}$ ), 6.86 (m, 4H, DMT), 7.45–7.17 (m, 9H, DMT), 7.83 (s, 1H,  $\text{CH}_{\text{ar}}$ ), 7.90 (s, 1H,  $\text{CH}_{\text{ar}}$ ), 11.37 (s, 1H, NH).

$^{13}\text{C}$  NMR (75 MHz,  $\text{CDCl}_3$ ):  $\delta$  (ppm) = 29.71 ( $\text{CH}_3$ ), 45.79 ( $\text{CH}_2\text{-N}$ ), 55.26 ( $\text{CH}_3\text{-O}$ , DMT), 68.58 ( $\text{CH-O}$ ), 76.65 ( $\text{CH-O}$ ), 77.23 ( $\text{CH-O}$ ), 81.43 (C, DMT), 113.16 ( $\text{CH}_{\text{ar}}$ ), 127.09–129.12 ( $\text{CH}_{\text{ar}}$ , DMT), 139.43 ( $\text{C}_{\text{ar}}$ ), 147.30–158.61 ( $\text{C}_{\text{ar}}$ , DMT), 159.40 ( $\text{C}_{\text{ar}}$ ).

1-(Bis(4-methoxyphenyl) (phenyl)methoxy)-5-(7,8-dimethyl-2,4-dioxo-3,4-dihydrobenzo[g]pteridin-10(2H)-yl)pentane-

2,3,4-triyl triacetate (Compound 2). This was synthesized as described previously.<sup>26</sup> In brief, compound 1 (510 mg, 0.75 mmol) was dissolved in dry pyridine (75 mL) and then cooled in an ice bath under argon atmosphere. Acetic anhydride (40 equiv, 2.8 mL, 30 mmol) was added dropwise and the reaction mixture was stirred overnight in the dark at rt. To stop the reaction 3 mL of methanol were added and organic solvents were evaporated under reduced pressure. The crude product was purified by silica gel column chromatography (Ethyl acetate/Hexane 8/2) to give the desired compound as orange solid. Yield: 545 mg (0.68 mmol, 90%).

$^1\text{H}$  NMR (300 MHz,  $\text{DMSO}-d_6$ ):  $\delta$  (ppm) = 1.49 (s, 3H,  $\text{CH}_3$ , Ac), 2.01 (s, 3H,  $\text{CH}_3$ , Ac), 2.27 (s, 3H,  $\text{CH}_3$ , Ac), 2.39 (s, 3H,  $\text{CH}_3$ ), 2.41 (s, 3H,  $\text{CH}_3$ ), 3.08–3.03 (m, 1H,  $\text{CH}_2\text{-O}$ ), 3.26–3.22 (m, 1H,  $\text{CH}_2\text{-O}$ ), 3.73 (s, 6H,  $2 \times \text{CH}_3\text{-O}$ , DMT), 4.79 (s, 1H,  $\text{CH}_2\text{-N}$ ), 4.84 (s, 1H,  $\text{CH}_2\text{-N}$ ), 5.25 (m, 2H,  $\text{CH-O}$ ), 5.49 (m, 1H,  $\text{CH-O}$ ), 6.87 (m, 4H, DMT), 7.33–7.2 (m, 9H, DMT), 7.65 (s, 1H,  $\text{CH}_{\text{ar}}$ ), 7.90 (s, 1H,  $\text{CH}_{\text{ar}}$ ), 11.42 (s, 1H, NH).

$^{13}\text{C}$  NMR (75 MHz,  $\text{CDCl}_3$ ):  $\delta$  (ppm) = 19.36 ( $\text{CH}_3$ ), 20.34 ( $\text{CH}_3$ , Ac), 21.13 ( $\text{CH}_3$ , Ac), 21.40 ( $\text{CH}_3$ , Ac), 45.17 ( $\text{CH}_2\text{-N}$ ), 55.19 ( $\text{CH}_3\text{-O}$ , DMT), 60.78 ( $\text{CH}_2\text{-O}$ ), 62.49 ( $\text{CH-O}$ ), 70.14 ( $\text{CH-O}$ ), 72.45 ( $\text{CH-O}$ ), 81.30 (C, DMT), 113.12 ( $\text{CH}_{\text{ar}}$ , DMT), 115.73 ( $\text{CH}_{\text{ar}}$ ), 126.86–131.39 ( $\text{CH}_{\text{ar}}$ , DMT), 132.49 ( $\text{CH}_{\text{ar}}$ ), 132.61 ( $\text{CH}_{\text{ar}}$ , DMT), 134.57 ( $\text{C}_{\text{ar}}$ ), 134.67 ( $\text{C}_{\text{ar}}$ ), 135.49–139.52 ( $\text{C}_{\text{ar}}$ , DMT), 144.41 ( $\text{C=N}$ ), 148.15–158.52 ( $\text{C}_{\text{ar}}$ , DMT), 159.61 ( $\text{C=O}$ ), 170.12 ( $\text{C=O}$ , Ac), 170.33 ( $\text{C=O}$ , Ac), 170.62 ( $\text{C=O}$ , Ac).

1-(7,8-Dimethyl-2,4-dioxo-3,4-dihydrobenzo[g]pteridin-10(2H)-yl)-5-hydroxypentane-2,3,4-triyl triacetate (Compound 3). This was synthesized as described previously.<sup>26</sup> Compound 2 (545 mg, 0.68 mmol) was dissolved in 20 mL nitromethane and 1.27 g (9 equiv, 5.6 mmol) of anhydrous  $\text{ZnBr}_2$  were added. After 10 min the reaction was quenched by addition of ammonium acetate (100 mL, 1 M in water). Then, 100 mL of DCM was added and the organic layer was separated, washed with brine ( $2 \times 40$  mL), and dried with sodium sulfate. After evaporation of DCM under reduced pressure, the crude product was extracted several times with ice-cold diethyl ether to remove residual DMT. The desired compound was obtained as yellow powder (323 mg) and utilized for the next step without further purification.

1-(((2-Cyanoethoxy) (diisopropylamino)phosphanyl)oxy)-5-(7,8-dimethyl-2,4-dioxo-3,4-dihydrobenzo[g]pteridin-10(2H)-yl)pentane-2,3,4-triyl triacetate (Compound 4). All starting materials were dried overnight under high vacuum. The glassware and molecular sieves were dried overnight in oven at  $200^\circ\text{C}$ . Under argon atmosphere compound 3 (323 mg) was dissolved in 6 mL of dry DCM containing molecular sieves. To this solution freshly distilled DIPEA (0.55 mL) and 2-cyanoethyl-*N,N*-diisopropylchlorophosphoramidite (1.2 equiv, 0.17 mL, 0.78 mmol) were added. After overnight stirring at rt, the reaction was stopped with 0.5 mL of methanol. The reaction mixture was evaporated under reduced pressure, then diluted in ethyl acetate (10 mL) with TEA (0.5 mL) and washed with brine ( $2 \times 20$  mL). Combined organic layers were dried with sodium sulfate and solvents were removed under reduced pressure. The presence of desired compound was confirmed by  $^{31}\text{P}$  NMR and ESI-MS analysis with sufficient purity and the crude product (241 mg) was utilized without purification. Prior to the next reaction step the product was stored overnight in a vacuum desiccator with phosphorus pentoxide.

$^{31}\text{P}$  NMR (121 MHz,  $\text{CDCl}_3$ ): two diastereoisomers  $\delta$  (ppm) = 152.29, 152.47.

Mass calculated: 702.7; found: 701.3 ( $\text{M}^{-1}$ ) (Figure S6).

(*S*)-4-((4-methoxyphenoxy)methyl)-2,2-dimethyl-1,3-dioxolane (Compound 5). (*S*)-(+)-1,2-Isopropylidenglycerol (0.96 mL 7.50 mmol), paramethoxyphenol (3 equiv, 2.79 g, 22.5 mmol) and triphenylphosphine (1.3 equiv, 2.56 g, 9.75 mmol) were dissolved in dry toluene (35 mL). Then diethylazodicarboxylate 40% in toluene (1.3 equiv, 4.4 mL, 9.75 mmol) was added dropwise. After stirring 3 h at rt, the reaction mixture was diluted in water. The aqueous layer was extracted with diethyl ether ( $2 \times 10$  mL) and the combined organic layers were washed with brine ( $2 \times 15$  mL), dried over sodium sulfate, and removed under reduced pressure. The crude product was purified by silica gel chromatography (ethyl acetate/hexane 10/90) to afford the desired product as yellow oil (1.69 g, 94%).

$^1\text{H}$  NMR (300 MHz,  $\text{CDCl}_3$ ):  $\delta$  (ppm) = 1.40 (s, 3H,  $\text{CH}_3$ ), 1.41 (s, 3H,  $\text{CH}_3$ ), 3.77 (s, 3H,  $\text{CH}_3\text{-O}$ , PMP), 3.89 (dd,  $J$  = 8.8; 5.9 Hz, 2H,  $\text{CH}_2\text{-O}$ ), 4.01 (dd,  $J$  = 9.5; 5.5 Hz, 1H,  $\text{CH-O}$ ), 4.13–4.20 (m, 1H,  $\text{CH}_2\text{-O}$ ), 4.50–4.43 (m, 1H,  $\text{CH}_2\text{-O}$ ), 6.84 (m, 4H,  $\text{CH}_{\text{ar}}$ ).

$^{13}\text{C}$  NMR (75 MHz,  $\text{CDCl}_3$ ):  $\delta$  (ppm) = 25.38 ( $\text{CH}_3$ ), 26.81 ( $\text{CH}_3$ ), 55.72 ( $\text{CH}_3\text{-O}$ , PMP), 66.87 ( $\text{CH}_2\text{-O}$ ), 69.50 ( $\text{CH}_2\text{-O}$ ), 77.24 ( $\text{CH-O}$ ), 109.71 (C), 115.47 ( $\text{CH}_{\text{ar}}$  PMP), 152.70 ( $\text{C}_{\text{ar}}$  PMP), 154.03 ( $\text{C}_{\text{ar}}$  PMP).

(*R*)-3-(4-Methoxyphenoxy)propane-1,2-diol (Compound 6). Compound 5 (1.69 g, 7.0 mmol) was dissolved in methanol (50 mL) and DOWEX 50 H+ resin (3.30 g) was added. The reaction mixture was stirred overnight at rt then filtered and methanol was evaporated under reduced pressure. TLC (ethyl acetate/hexane 70:30) and  $^1\text{H}$  NMR analysis of crude product showed the desired compound with sufficient purity. The product (1.32 g, white powder) was utilized without further purification.

$^1\text{H}$  NMR (300 MHz,  $\text{CDCl}_3$ ):  $\delta$  (ppm) = 3.69–3.88 (m, 5H,  $\text{CH}_3\text{-O}$ ,  $\text{CH}_2\text{-O}$ ), 3.94–4.02 (m, 2H,  $\text{CH}_2\text{-O}$ ), 4.05–4.12 (m, 1H,  $\text{CH-O}$ ), 6.84 (m, 4H,  $\text{CH}_{\text{ar}}$ ).

$^{13}\text{C}$  NMR (75 MHz,  $\text{CDCl}_3$ ):  $\delta$  (ppm) = 55.72 ( $\text{CH}_3\text{-O}$ , PMP), 63.70 ( $\text{CH}_2\text{-O}$ ), 69.89–70.46 ( $\text{CH}_2\text{-O}$ ), 77.25 ( $\text{CH-O}$ ), 114.67 ( $\text{CH}_{\text{ar}}$  PMP), 115.47 ( $\text{CH}_{\text{ar}}$  PMP), 152.70 ( $\text{C}_{\text{ar}}$  PMP), 154.03 ( $\text{C}_{\text{ar}}$  PMP).

(*S*)-1-(2,3-Bis(tetradecyloxy)propoxy)-4-methoxybenzene (Compound 7). PMP-protected compound 6 (1.32 g) was added to a suspension of NaH 60% (4 equiv, 0.89 g, 26.6 mmol) in dry DMF (67 mL). After stirring for 30 min at rt, 1-bromotetradecane (6 equiv, 12 mL, 39.9 mmol) was slowly added. The reaction mixture was stirred overnight at room temperature. To stop the reaction 20 mL of MeOH were added and the crude product was diluted with water. The aqueous layer was extracted with diethyl ether ( $3 \times 20$  mL) and the combined organic layers were washed with brine ( $2 \times 30$  mL), dried over sodium sulfate, and removed under reduced pressure. The crude product was purified by silica gel chromatography (hexane/ethyl acetate 90/10) to afford the desired product as a white solid (2.73 g, 66%).

$^1\text{H}$  NMR (300 MHz,  $\text{CDCl}_3$ ):  $\delta$  (ppm) = 0.86 (m, 6H,  $2 \times \text{CH}_3$ ), 1.25 (s, 44H,  $22 \times \text{CH}_2$ ), 1.59 (m, 4H,  $2 \times \text{CH}_2$ ), 3.38–3.65 (m, 6H,  $3 \times \text{CH}_2\text{-O}$ ), 3.70–3.79 (m, 4H,  $\text{CH}_3\text{-O}$ ,  $\text{CH-O}$ ), 3.93–4.06 (m, 2H,  $\text{CH}_2\text{-O}$ ), 6.82 (m, 4H,  $\text{CH}_{\text{ar}}$ ).

$^{13}\text{C}$  NMR (75 MHz,  $\text{CDCl}_3$ ):  $\delta$  (ppm) = 14.17 ( $\text{CH}_3$ ), 22.73–31.95 ( $\text{CH}_2$ ), 55.70 ( $\text{CH}_3\text{-O}$ , PMP), 68.64 ( $\text{CH}_2\text{-O}$ ), 70.37 ( $\text{CH}_2\text{-O}$ ), 70.81 ( $\text{CH}_2\text{-O}$ ), 71.75 ( $\text{CH}_2\text{-O}$ ), 77.23

( $\text{CH-O}$ ), 114.51 ( $\text{CH}_{\text{ar}}$  PMP), 115.53 ( $\text{CH}_{\text{ar}}$  PMP), 153.06 ( $\text{C}_{\text{ar}}$  PMP), 153.78 ( $\text{C}_{\text{ar}}$  PMP).

(*R*)-2,3-Bis(tetradecyloxy)propan-1-ol (Compound 8). Compound 7 2.73 g (4.62 mmol) was dissolved in ACN/ $\text{H}_2\text{O}$  8:2 mixture (45 mL) and then put on ice bath. 6.65 g of ceric ammonium nitrate (2.6 equiv, 12 mmol) were added subsequently and the reaction mixture was stirred overnight. After a workup procedure (brine  $2 \times 30$  mL, sodium sulfate) the crude product was purified by silica gel chromatography (hexane/ethyl acetate 90/10) to give a white powder (1.37 g, 61%) (NMR spectra, Figures S5–7).

$^1\text{H}$  NMR (300 MHz,  $\text{CDCl}_3$ ):  $\delta$  (ppm) = 0.88 (m, 6H,  $2 \times \text{CH}_3$ ), 1.25 (s, 44H,  $22 \times \text{CH}_2$ ), 1.57 (m, 4H,  $2 \times \text{CH}_2$ ), 2.01 (s, 1H, OH), 3.41–3.75 (m, 9H,  $4 \times \text{CH}_2\text{-O}$ ,  $\text{CH-O}$ ).

$^{13}\text{C}$  NMR (75 MHz,  $\text{CDCl}_3$ ):  $\delta$  (ppm) = 14.14 ( $\text{CH}_3$ ), 22.71–31.94 ( $\text{CH}_2$ ), 63.11 ( $\text{CH}_2\text{-OH}$ ), 70.40 ( $\text{CH}_2\text{-O}$ ), 70.91 ( $\text{CH}_2\text{-O}$ ), 71.86 ( $\text{CH}_2\text{-O}$ ), 77.22 ( $\text{CH}_2\text{-O}$ ), 78.21 ( $\text{CH-O}$ ).

Mass calculated: 484.8; found: 485.5 ( $\text{M}^{+1}$ ) (Figure S8).

1-(((*S*)-2,3-Bis(tetradecyloxy)propoxy)(2-cyanoethoxy)phosphoryl)oxy)-5-(7,8-dimethyl-2,4-dioxo-3,4-dihydrobenzo[*g*]pteridin-10(2H)-yl)pentane-2,3,4-triyl triacetate (Compound 9). To afford compound 9 all starting materials were dried overnight in a high vacuum pump. The glassware and molecular sieves were dried overnight in an oven at 200 °C. Under argon atmosphere compound 4 (241 mg) was dissolved in 3 mL dry THF containing molecular sieves. Then a solution of 200 mg diC14 alcohol (1.2 equiv, 0.41 mmol) in 3 mL THF and 4.4 mL of 5-benzylthio-1H-tetrazole (1.3 equiv, 0.44 mmol) were added. After stirring 6 h at RT, 20 mL of an oxidizing solution (0.2 M iodine in THF/Pyridine/ $\text{H}_2\text{O}$  (2:1:1)) was added. The reaction was stirred overnight at rt and stopped by adding a solution of sodium bisulfite (5% in water) until the brown color had vanished. The reaction mixture was diluted with ethyl acetate (20 mL) and the organic layer was washed with sodium bicarbonate ( $2 \times 20$  mL) and brine ( $2 \times 20$  mL) and finally dried with sodium sulfate. The solvents were evaporated under reduced pressure. The crude product was purified by silica gel column chromatography (ethyl acetate 100%) to afford a yellow powder. Yield: 227 mg (0.21 mmol, 30%).

$^1\text{H}$  NMR (300 MHz,  $\text{CDCl}_3$ ):  $\delta$  (ppm) = 0.87 (t,  $J$  = 6.6 Hz, 6H,  $2 \times \text{CH}_3$ , chains), 1.24 (s, 44H,  $22 \times \text{CH}_2$ , chains), 1.52 (m, 4H,  $2 \times \text{CH}_2$ , chains), 1.79 (s, 3H,  $\text{CH}_3$ , Ac), 2.20 (s, 3H,  $\text{CH}_3$ , Ac), 2.34 (s, 3H,  $\text{CH}_3$ , Ac), 2.44 (s, 3H,  $\text{CH}_3$ ), 2.58 (s, 3H,  $\text{CH}_3$ ), 2.80 (t,  $J$  = 6.1 Hz, 2H,  $\text{CH}_2\text{-CN}$ ), 3.37–3.46 (m, 2H,  $\text{CH}_2\text{-O}$ ), 3.49 (m, 2H,  $\text{CH}_2\text{-O}$ ), 3.55 (m, 2H,  $\text{CH}_2\text{-O}$ ), 3.55 (m, 1H,  $\text{CH-O}$ ), 4.49–4.03 (m, 7H,  $3 \times \text{CH}_2\text{-O}$ ,  $1 \times \text{CH}_2\text{-N}$ ), 4.87 (m,  $\text{CH}_2\text{-N}$ ), 5.41 (m, 1H,  $\text{CH-O}$ ), 5.49 (m, 1H,  $\text{CH-O}$ ), 5.62 (m, 1H,  $\text{CH-O}$ ), 7.60 (s, 1H), 8.03 (s, 1H), 8.39 (s, 1H, NH).

$^{13}\text{C}$  NMR (75 MHz,  $\text{CDCl}_3$ ):  $\delta$  (ppm) = 14.11 ( $\text{CH}_3$ , chains), 19.42 ( $\text{CH}_3$ ), 20.33 ( $\text{CH}_3$ , Ac), 21.09 ( $\text{CH}_3$ , Ac), 21.42 ( $\text{CH}_3$ , Ac), 22.67–31.90 ( $\text{CH}_2$ , chains), 45.10 ( $\text{CH}_2\text{-N}$ ), 62.27 ( $\text{CH}_2\text{-O}$ ), 67.88 ( $\text{CH}_2\text{-O}$ ), 69.35 ( $\text{CH}_2\text{-O}$ ), 70.20 ( $\text{CH}_2\text{-O}$ ), 70.70 ( $\text{CH}_2\text{-O}$ ), 71.84 ( $\text{CH}_2\text{-O}$ ), 76.95 ( $\text{CH-O}$ ), 77.29 ( $\text{CH-O}$ ), 115.71 ( $\text{CH}_{\text{ar}}$ ), 116.61 ( $\text{CH}_{\text{ar}}$ ), 128.65 ( $\text{CH}_{\text{ar}}$ ), 129.06–137.05 ( $\text{C}_{\text{ar}}$ ), 148.29 ( $\text{C=N}$ ), 154.83 ( $\text{C=N}$ ), 159.29 ( $\text{C=O}$ ), 169.88 ( $\text{C=O}$ , Ac), 170.23 ( $\text{C=O}$ , Ac), 170.26 ( $\text{C=O}$ , Ac).

$^{31}\text{P}$  NMR (121 MHz,  $\text{CDCl}_3$ ): two diastereoisomers  $\delta$  (ppm) = 1.88, 1.98.

Mass calculated: 1102.4; found: 1102.6.

(*S*)-2,3-Bis(tetradecyloxy)propyl (5-(7,8-dimethyl-2,4-dioxo-3,4-dihydrobenzo[*g*]pteridin-10(2*H*)-yl)-2,3,4-trihydroxypentyl) phosphate (Compound **10**, *RfdiC14*). Compound **9** (227 mg, 0.21 mmol) was dissolved in 5 mL of methanol and 51 mg of sodium methanoate (3.5 equiv, 0.75 mmol) were added. After 24 h stirring at rt the reaction was stopped by the addition of 4 g of dry silica. The solvent was evaporated under reduced pressure and the crude product was purified by silica gel column chromatography (DCM/MeOH/TEA 95/5/1) to afford yellow powder. Yield: 151 mg (0.17 mmol, 80%) (NMR spectra, Figures S1–S4).

<sup>1</sup>H NMR (400 MHz, CDCl<sub>3</sub>/MeOD 2:1):  $\delta$  (ppm) = 0.84 (t, *J* = 6.7 Hz, 6H, 2  $\times$  CH<sub>3</sub>, chains), 1.22 (s, 44H, 22  $\times$  CH<sub>2</sub>, chains), 1.31 (TEA, t, *J* = 7.3 Hz, 9H, 3  $\times$  CH<sub>3</sub>), 1.53 (m, 4H, 2  $\times$  CH<sub>2</sub>, chains), 2.42 (s, 3H, CH<sub>3</sub>), 2.53 (s, 3H, CH<sub>3</sub>), 3.13 (TEA, q, *J* = 7.3 Hz, 6H, 3  $\times$  CH<sub>2</sub>), 3.35–3.62 (m, 9H, 4  $\times$  CH<sub>2</sub>–O, CH–O, chains), 3.81–3.95 (m, 4H, 2  $\times$  CH<sub>2</sub>–O), 4.12 (m, 1H, CH–O), 4.81 (m, 1H, CH–O), 4.93 (m, 1H, CH<sub>2</sub>–N), 5.13 (m, 1H, CH<sub>2</sub>–N), 7.96 (m, 2H, CH<sub>ar</sub>).

<sup>13</sup>C NMR (100 MHz, CDCl<sub>3</sub>/MeOD 2:1):  $\delta$  (ppm) = 8.81 (CH<sub>2</sub>, TEA), 14.26 (CH<sub>3</sub>, chains), 19.57 (CH<sub>3</sub>), 21.56 (CH<sub>3</sub>), 23.01–32.27 (CH<sub>2</sub>, chains), 46.63 (CH<sub>2</sub>–N, TEA), 47.68 (CH<sub>2</sub>–N), 48.82 (CH<sub>2</sub>–N), 52.89 (CH<sub>2</sub>–O), 58.67 (CH<sub>2</sub>–O), 65.48 (CH<sub>2</sub>–O), 67.45 (CH<sub>2</sub>–O), 70.84–73.00 (CH<sub>2</sub>–O, CH–O, chains, RF), 77.95–78.35 (CH–O, chains, RF), 117.71 (CH<sub>ar</sub>), 132.09 (CH<sub>ar</sub>), 132.83 (C<sub>ar</sub>), 135.78 (C<sub>ar</sub>), 138.09 (C<sub>ar</sub>), 149.19 (C=N), 151.13 (C=N), 157.50 (C=O), 161.03 (C=O).

<sup>31</sup>P NMR (162 MHz, CDCl<sub>3</sub>): 1.86.

Mass calculated: 923.2; found: 923.5 (Figure S8).

**DSPE-PEG-riboflavin (Compound 11).** 400  $\mu$ L of stock solution (25 mg/mL in chloroform) of DSPE-PEG2000-succinyl (10 mg, 0.34  $\mu$ mol) were put in a round-bottom flask and the solvent was evaporated under gentle nitrogen stream. RF (20 equiv, 2.5 mg, 6.8  $\mu$ mol) was solubilized in anhydrous DMF and added to DSPE-PEG-succinyl. Then a catalytic amount of DMAP and a stoichiometric amount of DCC were added and the reaction mixture was left under N<sub>2</sub> and continuous magnetic stirring. After 48 h DMF was evaporated by lyophilization (Dura-DryMP from FTS Systems), the crude product was dissolved in H<sub>2</sub>O/ACN 50:50 mixture and purified by HPLC on reverse phase analytical C8 column. Solvent A was H<sub>2</sub>O/ACN/TFA 50:50:0.1 and solvent B was H<sub>2</sub>O/ACN/TFA 50:50:0.1, with the gradient from 0% to 100% B in 25 min and then 100–0% B in 5 min. The product was detected by the UV-detector at 265 nm. Gathered fractions were lyophilized and analyzed with MALDI-TOF mass spectrometry.

Mass observed: 3288; 2438.

**Liposome Preparation and Characterization.** *Preparation.* Liposomes were prepared with standard film hydration method. The final concentration of lipids was 20 mM. For the targeted liposomes at least 1 mol % of RF amphiphile was added to the initial lipid blend. For the NIR-labeled long-circulating liposomes DiR dye was added to the initial lipid blend (0.1 mol %). The lipids were dissolved in chloroform, mixed in appropriate proportions in the round-bottom flask, and the solvent evaporated under vacuo. The flask was then put into lyophilizer overnight to remove any residual solvent traces. The film was hydrated with 1 mL of 25 mM HEPES buffer (pH = 7.4) containing 1 mM of Rhodamine B (for 1 h at 40 °C) for bare liposomes or with 10 mM HEPES buffer (pH = 7.4) with 9.25% sucrose (for 1 h at 60 °C) for LCL. Hydrated

films were then subjected to 3–5 freeze–thaw cycles with the help of liquid nitrogen and a water bath (40–60 °C). Obtained MLV were then extruded 11 times through a 100 nm polycarbonate membrane (Avanti Polar Lipids). To separate liposomes from free Rhodamine B in solution, LUVs were purified by size-exclusion chromatography with prepacked PD10 columns (Sephadex G25 resin, GE Healthcare). The liposome purity and stability were evaluated by GPC with a help of BioSep-SEC-S3000 column (isocratic mode in PBS, flow rate 1 mL/min, 20 min). Liposome solutions were stored at 4 °C.

**Size and Charge Measurement.** Size, distribution, and zeta potential measurements of control and specific liposomes were performed in triplicate by dynamic light scattering (DLS) using a Zetasizer Nano ZS (Malvern Instruments Ltd., Malvern, Worcestershire, UK) at 25 °C. Calculations of size distribution based on light scattering intensity were performed by the Zetasizer Nano software from the correlation functions using the general purpose algorithm (Malvern dispersion technology software, v 7.03). The liposomal stock dispersions were diluted by a factor 15 with an appropriate HEPES buffer before measurements performed by DLS.

**Cryo-EM.** Cryo-EM analysis was performed as described earlier.<sup>41</sup> For the sample preparation, 5  $\mu$ L of sample aliquot was deposited onto an EM grid coated with a perforated carbon film (Ted Pella, Redding, CA, USA), the excess liquid was blotted off with a filter paper, and the grid was then quickly plunged into liquid ethane using a Leica EM-CPC cryo-chamber. EM grids were stored in cryo-boxes under liquid nitrogen until use, and then mounted in a Gatan 626 cryo-holder and transferred in a Tecnai F20 microscope operated at 200 kV. Images were recorded with a USC1000-SSCCD Gatan camera. The size of the objects was measured with ImageJ software (U.S. National Institutes of Health, Bethesda, Maryland, USA).

**Fluorescence Spectroscopy.** Liposome fluorescence intensity was evaluated by Tecan Infinite 200 Pro (Tecan Trading AG, Switzerland) and analyzed with Tecan i-control, v 1.7.1.12 software. First calibration curves were prepared for Riboflavin (ex. 450 nm, em. 530 nm), Rhodamine B (ex. 554 nm, em. 583 nm), and DiR (ex. 750 nm, em. 782 nm). The concentration of fluorescent agent in each batch of liposomes was determined with following equations:  $y = 59087x$  ( $R^2 = 0.9939$ ) for Riboflavin and  $y = 17888x$  ( $R^2 = 0.98918$ ) for Rhodamine B,  $y = 7200x$  ( $R^2 = 0.9916$ ) for DiR, where  $y$  represents fluorescence intensity and  $x$  the concentration in  $\mu$ M.

**Solid State NMR.** Two sets of samples were prepared: DMPC:DMPG (90:10) and DMPC:DMPG:RfdiC14 (90:10:10) with the total lipid concentration of 20 mM. For all samples DMPC-d54 (Avanti Polar Lipids, USA) with fully deuterated acyl chains was utilized. Lipids were dissolved in chloroform, mixed in appropriate proportions, and the solvent evaporated under gentle nitrogen stream. The obtained lipid films were taken up in 500  $\mu$ L of MiliQ water, hydrated at 45 °C for 30 min, and then subjected to 5 freeze–thaw cycles. After the last cycle samples were frozen in liquid nitrogen and lyophilized (Dura-DryMP from FTS Systems). The obtained powder was taken up in 100  $\mu$ L of light water (containing 2–3 ppm of deuterium, CortectNet, France) for solid NMR studies. Then again 3 freeze–thaw cycles occurred (10 min at 45 °C/stirring/freezing in liquid nitrogen) before the transfer to 4 mm zircon oxide rotors (CortectNet, France).



The NMR spectrometer RMN 800 MHz SB Bruker (Wissembourg, France) equipped with the probe CP-MAS SB  $^1\text{H}/\text{BB}$  able to rotate at magic angle was used for the solid NMR studies. The echo solid sequence ( $90^\circ\text{-}\tau\text{-}90^\circ\text{-}\tau\text{-Acq}$ ) was employed for the deuterium observations. The pulses at  $90^\circ$  were  $2.88\ \mu\text{s}$ , the echo delays ( $\tau$ ) were  $40\ \mu\text{s}$  with the registering from 4k points. The repeating time was 2 s with the acquisitions number from 1 to 12k according to the sample. The temperature varied from  $20$  to  $50 \pm 5\ ^\circ\text{C}$ . The obtained signals were filtered with a decreasing exponential function of the constant between 100 and 500 Hz and then subjected to Fourier transformation from the top of the echo spin. Finally, the data were analyzed with the help of Topspin 3.2 software (Bruker, USA).

**Cellular Uptake Experiments.** *Cell Culture.* A431 (human epidermal cervix carcinoma) and PC3 (human prostate carcinoma) cell lines as well as HUVEC (human umbilical vein endothelial cells) primary culture were maintained at  $37\ ^\circ\text{C}$ , under humidified air with  $5\%\ \text{CO}_2$ , in RMPI, McCoy's medium, or Endopan 3 L-Glutamine medium supplemented with  $10\%$  (v/v) fetal bovine serum (except HUVECs) and  $100\ \text{U/mL}$  of penicillin G and  $100\ \text{U/mL}$  of streptomycin (cell culture media and additives were from Gibco/Life Technologies, Carlsbad, California). Cells were cultivated in standard  $75\ \text{cm}^2$  flasks and splitted each 3–5 days (up to 10 passages maximum).

*Fluorescent Microscopy.* Cells in maintenance medium were trypsinized and seeded into 24-well culture plates at optimum confluence. Incubations were conducted at  $50\ \text{nM}$  (RhB) of control or targeted liposomes in serum-containing maintenance medium for 30 min. For the competitive binding experiment cells were preincubated with 20-fold excess of targeted liposomes without RhB for 15 min and then, without washing,  $50\ \text{nM}$  of targeted liposomes were added and incubated for 30 min. For  $4\ ^\circ\text{C}$  uptake studies cells were preincubated in the refrigerator for 30 min. After incubation with liposomes, cells were washed three times in  $1\times$  PBS to remove free liposomes and fixed with  $4\%$  PFA. The cell nucleus was stained with DAPI standard protocol (Life Technologies). Cellular uptake was monitored by fluorescence microscopy in on an AxioVert microscope (Carl Zeiss AG) under  $20\times$  or  $40\times$  magnification. Two channels were studied for each liposome batch—DAPI (ex.  $365\ \text{nm}$ , em.  $455\ \text{nm}$ ) to visualize nucleus and dsRed (ex.  $554\ \text{nm}$ , em.  $605\ \text{nm}$ ) to observe liposome uptake trough RhB fluorescence or Cy7 (ex.  $750\ \text{nm}$ , em.  $782\ \text{nm}$ ) for DiR fluorescence in LCL. For each individual well from 10 to 20 images were collected and the fluorescence intensity was then quantified with ImageJ Software (U.S. National Institutes of Health, Bethesda, Maryland, USA). Uptake experiments were conducted in triplicate.

*Flow Cytometry.* The incubation conditions were the same as for fluorescence microscopy experiments. Briefly, cells were trypsinized, counted, and then incubated in Eppendorf tubes ( $0.4\ \text{million cells/mL}$ ) with  $50\ \text{nM}$  of liposomes for 30 min at  $37\ ^\circ\text{C}$ . Then, tubes were centrifuged and the cell pellet was washed 3 times with PBS to remove free liposomes. For the competition experiment cells were preincubated with a 20-fold excess of targeted liposomes without Rhodamine B for 15 min. Finally, cells were resuspended in PBS buffer in flow cytometry tubes and the measurements were performed using a FACS Canto II (Becton Dickinson) flow cytometer. Fluorescence was monitored in two channels—green channel FITC (ex.  $495\ \text{nm}$ , em.  $519\ \text{nm}$ ) and orange channel—PE (ex.  $561\ \text{nm}$ , em.  $578$

$\text{nm}$ ).  $50\ 000$  cells were counted for each condition tested. The data were analyzed and quantified using FACS Diva Software (Becton Dickinson).

**Cytotoxicity Test.** The cytotoxicity of control and specific liposomes was accessed using a standard MTT (Life Technologies) test following the manufacturer's description. Briefly, cells in maintenance medium were seeded in 96 well plates and incubated for 72 h with liposomes in  $1\times$ ,  $3\times$ , and  $5\times$  concentrations ( $50$ ,  $150$ , and  $250\ \text{nM}$ , respectively). After incubation, cells were washed with maintenance medium without serum and  $50\ \mu\text{L}$  of MTT ( $5\ \text{mg/mL}$ ) solution per well was added. Cells were incubated 2 h at  $37\ ^\circ\text{C}$  and the MTT solution was removed. Formed by live cells, blue formazan crystals were solubilized with  $200\ \mu\text{L}$  DMSO per well. The blue formazan absorbance was read at  $570\ \text{nm}$  with Tecan Infinite 200 Pro. The cell viability was calculated using the following formula: Viability % =  $(A_{570\ \text{nm}}$  for the treated cells/ $A_{570\ \text{nm}}$  for the control cells)  $\times 100\%$ , where  $A_{570\ \text{nm}}$  is the absorbance value. Each assay was repeated in triplicate.

**In Vivo Experiments.** The in vivo experiments were approved by the local and national regulatory authorities and by ethical animal welfare committee under the number AZ - 87-51.04.2010.A278. Eight-week old male CD1-nu/nu mice (Charles River Laboratories, Wilmington, USA) weighing  $\sim 25\ \text{g}$  were fed with chlorophyll-free food pellets and water ad libitum. Mice were housed in ventilated cages and placed in controlled room with adapted conditions. PC3 human prostate carcinoma cells were cultured as described in [Cell Culture](#). Mice were injected with PC3 tumor cells ( $3 \times 10^6$  cells/ $100\ \mu\text{L}$ ) by subcutaneous inoculation into the dorsolateral right flank. A tumor size of  $\sim 3\text{--}4\ \text{mm}$  in diameter was obtained within 30–40 days. The animals were conditionally inhalation-anaesthetized during all experimental operations.

**Phantom Studies.** Phantom studies for the probe calibration were performed in a block shaped FMT phantom<sup>36</sup> ( $33 \times 40 \times 15\ \text{mm}^3$ , absorption  $0.1\ \text{cm}^{-1}$ , scattering  $8\ \text{cm}^{-1}$ ), containing a cylindrical inclusion (diameter  $3\ \text{mm}$ , length  $1\ \text{cm}$ ). The inclusion was filled with varying concentrations of fluorescent DiR liposomes (ex  $750\ \text{nm}$ , em  $782\ \text{nm}$ ).  $5\%$  CT contrast agent (Imeron 400, Bracco Imaging, Konstanz, Germany) was added to liposome solutions to facilitate the segmentation of the inclusion in the  $\mu\text{CT}$  images.  $1\%$  of Lipovenoes ( $20\%$  stock) were also added to mimic tissue absorption. The phantom was subjected to the  $\mu\text{CT}$  imaging (Tomoscope DUO;  $\mu\text{CT}$  Imaging, Erlangen, Germany) with subsequent 3D FMT scans (FMT2500; PerkinElmer). Based on  $\mu\text{CT}$  data, the cylindrical inclusion in phantom was segmented using Imalytics Preclinical (Gremse-IT, Aachen, Germany)<sup>42</sup> and the fluorescence signal from FMT was quantified in the segmented volume.

**Animal Studies.** Control and targeted LCL ( $100\ \mu\text{L}$  with  $2.5\ \text{nmol}$  DiR in each) were injected into the tail vein of 6 CD-1 nude male mice bearing PC3 tumors of size of  $\sim 3\text{--}4\ \text{mm}$  in diameter. Animals were divided in 2 groups—control and targeted with  $n = 3$  in each group. The anaesthetized ( $2.5\%$  mixture of isoflurane/ $\text{O}_2$ ) animals were placed on a multimodal imaging mice holder (CT-imaging, Erlangen, Germany), which is manually adjusted to keep the mice with the tumors projecting at the right side. High-resolution dual-energy  $\mu\text{CT}$  and subsequent image reconstruction were performed as described previously.<sup>38</sup> After the  $\mu\text{CT}$  scan, without changing the position and orientation of mouse, it was transferred to the FMT. Process parameters such as excitation wavelength and



calibration agent were preset by the FMT based on earlier phantom experiments. The FMT machine detected and set automatically the laser scanning depth of imaging holder. Whole body images of the mice were first captured using FRI. The 3D FMT scans were subsequently performed in the region of interest selected from 2D FRI images. All animals were subjected to  $\mu$ CT and subsequent 3D FMT imaging at 0.25, 4, 24, and 48 h. After the final scanning, Rhodamine-lectin (Axxora, LLC, 1 mg/mL; 70  $\mu$ L) was injected into the tail vein, and mice were sacrificed for ex vivo biodistribution validation. The  $\mu$ CT and FMT image data sets were fused as described previously.<sup>36</sup> Based on  $\mu$ CT data, tumors and healthy organs were interactively segmented using Imalytics Preclinical.<sup>42</sup> Fluorescence signals from FMT were overlaid with corresponding organ-segmented  $\mu$ CT images, and the concentration of control and targeted LCL in organs was quantified. The mean DiR content for each segmented organ was calculated on the basis of phantom experiments and was normalized to its respective average volume. The blood samples of 3  $\mu$ L per mouse were collected before injection and at 0.25, 4, 24, and 48 h after injection and placed at the filter paper. At the end of the experiment the filter paper was imaged with 2D FRI and fluorescence signal in each blood spot was quantified.

**Tumor Cryosections and Staining.** Histological stainings were performed to visualize the tumor micromorphology and compare the tumor accumulation of different liposomal formulations. Thus, snap-frozen 8- $\mu$ m-thick sections were prepared and stained using DAPI (Sigma-Aldrich, Germany) for nuclei. Blood vessels were already stained with Rhodamine-lectin. Sections were mounted on microscopy slides, washed twice with PBS and fixed using Mowiol (Sigma-Aldrich, Germany). Fluorescence microscopy imaging was performed using an Axio Imager M2 microscope and a high-resolution AxioCam MRm Rev.3 camera, at different magnifications. The images were acquired in various positions of the tumor and within various depths. The data were further post-processed using ImageJ software (U.S. National Institutes of Health, Bethesda, Maryland, USA) and the colocalization was analyzed with Fiji Colocalization Test tool (U.S. National Institutes of Health, Bethesda, Maryland, USA).

**Statistics.** All data are presented as the mean  $\pm$  standard deviation. Two-tail Student's test and variance analysis were used to determine significance among groups. A value of  $P < 0.05$  was considered to show significant differences.

## ■ ASSOCIATED CONTENT

### ■ Supporting Information

The Supporting Information is available free of charge on the ACS Publications website at DOI: 10.1021/acs.bioconjchem.6b00317.

NMR and MS spectra and all additional experiments (PDF)

## ■ AUTHOR INFORMATION

### Corresponding Authors

\*E-mail: fkiessling@ukaachen.de.

\*E-mail: isabelle.berque-bestel@u-bordeaux.fr.

### Notes

The authors declare no competing financial interest.

## ■ ACKNOWLEDGMENTS

This work was supported by the Helmholtz-Society Portfolio grant "Technologie und Medizin – Multimodale Bildgebung zur Aufklärung des In-vivo-Verhaltens von polymeren Biomaterialien", by the Ligue Nationale contre le cancer, the Initiative d'Excellence and TGIR funding from University of Bordeaux, and by a START grant. The authors also greatly acknowledge Dr. Erick J Dufourc and Axelle Grelard for the NMR analysis of RfdiC14 samples and Dr. Boutayna Frih for the MALDI-TOF-TOF analysis of DSPE-PEG-RF.

## ■ REFERENCES

- (1) Riboflavin. Monograph. (2008) *Altern. Med. Rev. J. Clin. Ther.* 13, 334–340.
- (2) Jayapaul, J., Hodenius, M., Arns, S., Lederle, W., Lammers, T., Comba, P., Kiessling, F., and Gaetjens, J. (2011) FMN-coated fluorescent iron oxide nanoparticles for RCP-mediated targeting and labeling of metabolically active cancer and endothelial cells. *Biomaterials* 32, 5863–5871.
- (3) Thomas, T. P., Choi, S. K., Li, M.-H., Kotlyar, A., and Baker, J. R. (2010) Design of riboflavin-presenting PAMAM dendrimers as a new nanopatform for cancer-targeted delivery. *Bioorg. Med. Chem. Lett.* 20, 5191–5194.
- (4) Witte, A. B., Leistra, A. N., Wong, P. T., Bharathi, S., Refior, K., Smith, P., Kaso, O., Sinniah, K., and Choi, S. K. (2014) Atomic Force Microscopy Probing of Receptor–Nanoparticle Interactions for Riboflavin Receptor Targeted Gold–Dendrimer Nanocomposites. *J. Phys. Chem. B* 118, 2872–2882.
- (5) Bairi, P., Chakraborty, P., Mondal, S., Roy, B., and Nandi, A. K. (2014) A thixotropic supramolecular hydrogel of adenine and riboflavin-5'-phosphate sodium salt showing enhanced fluorescence properties. *Soft Matter* 10, 5114–5120.
- (6) Ju, S.-Y., and Papadimitrakopoulos, F. (2008) Synthesis and redox behavior of flavin mononucleotide-functionalized single-walled carbon nanotubes. *J. Am. Chem. Soc.* 130, 655–664.
- (7) Jayapaul, J., Arns, S., Lederle, W., Lammers, T., Comba, P., Gätjens, J., and Kiessling, F. (2012) Riboflavin carrier protein-targeted fluorescent USPIO for the assessment of vascular metabolism in tumors. *Biomaterials* 33, 8822–8829.
- (8) Mertens, M. E., Frese, J., Bölükbas, D. A., Hrdlicka, L., Golombek, S., Koch, S., Mela, P., Jockenhövel, S., Kiessling, F., and Lammers, T. (2014) FMN-coated fluorescent USPIO for cell labeling and non-invasive MR imaging in tissue engineering. *Theranostics* 4, 1002–1013.
- (9) Iida, H., Miki, M., Iwahana, S., and Yashima, E. (2014) Riboflavin-based fluorogenic sensor for chemo- and enantioselective detection of amine vapors. *Chem. - Eur. J.* 20, 4257–4262.
- (10) Pang, Y., Xu, Z., Sato, Y., Nishizawa, S., and Teramae, N. (2012) Base pairing at the basic site in DNA duplexes and its application in adenosine aptasensors. *ChemBioChem* 13, 436–442.
- (11) Iida, H., Iwahana, S., Mizoguchi, T., and Yashima, E. (2012) Main-Chain Optically Active Riboflavin Polymer for Asymmetric Catalysis and Its Vapochromic Behavior. *J. Am. Chem. Soc.* 134, 15103–15113.
- (12) Bairi, P., Roy, B., and Nandi, A. K. (2012) A light harvesting Bi-component hydrogel with a riboflavin acceptor. *Chem. Commun.* 48, 10850–10852.
- (13) Manna, S., Saha, A., and Nandi, A. K. (2006) A two component thermoreversible hydrogel of riboflavin and melamine: Enhancement of photoluminescence in the gel form. *Chem. Commun.*, 4285–4287.
- (14) Bairi, P., Roy, B., Chakraborty, P., and Nandi, A. K. (2013) Co-assembled white-light-emitting hydrogel of melamine. *ACS Appl. Mater. Interfaces* 5, 5478–5485.
- (15) Beztinna, N., Solé, M., Taib, N., and Bestel, I. (2016) Bioengineered riboflavin in nanotechnology. *Biomaterials* 80, 121–133.
- (16) Yao, Y., Yonezawa, A., Yoshimatsu, H., Masuda, S., Katsura, T., and Inui, K.-I. (2010) Identification and comparative functional

characterization of a new human riboflavin transporter hRFT3 expressed in the brain. *J. Nutr.* 140, 1220–1226.

(17) Yonezawa, A., Masuda, S., Katsura, T., and Inui, K. (2008) Identification and functional characterization of a novel human and rat riboflavin transporter, RFT1. *Am. J. Physiol. Cell Physiol.* 295, C632–641.

(18) Subramanian, V. S., Subramanya, S. B., Rapp, L., Marchant, J. S., Ma, T. Y., and Said, H. M. (2011) Differential expression of human riboflavin transporters -1, -2, and -3 in polarized epithelia: A key role for hRFT-2 in intestinal riboflavin uptake. *Biochim. Biophys. Acta, Biomembr.* 1808, 3016–3021.

(19) Yonezawa, A., and Inui, K. (2013) Novel riboflavin transporter family RFVT/SLC52: identification, nomenclature, functional characterization and genetic diseases of RFVT/SLC52. *Mol. Aspects Med.* 34, 693–701.

(20) Tsvetkova, Y., Beztsinna, N., Jayapaul, J., Weiler, M., Arns, S., Shi, Y., Lammers, T., and Kiessling, F. (2016) Refinement of adsorptive coatings for fluorescent riboflavin-receptor-targeted iron oxide nanoparticles. *Contrast Media Mol. Imaging* 11, 47.

(21) Holladay, S. R., Yang, Z., Kennedy, M. D., Leamon, C. P., Lee, R. J., Jayamani, M., Mason, T., and Low, P. S. (1999) Riboflavin-mediated delivery of a macromolecule into cultured human cells. *Biochim. Biophys. Acta, Gen. Subj.* 1426, 195–204.

(22) Chang, H.-I., and Yeh, M.-K. (2011) Clinical development of liposome-based drugs: formulation, characterization, and therapeutic efficacy. *Int. J. Nanomed.* 7, 49–60.

(23) Monaco, H. L. (1997) Crystal structure of chicken riboflavin-binding protein. *EMBO J.* 16, 1475–1483.

(24) Witte, A. B., Timmer, C. M., Gam, J. J., Choi, S. K., Banaszak Holl, M. M., Orr, B. G., Baker, J. R., and Sinniah, K. (2012) Biophysical characterization of a riboflavin-conjugated dendrimer platform for targeted drug delivery. *Biomacromolecules* 13, 507–516.

(25) Marlin, F., Simon, P., Bonneau, S., Alberti, P., Cordier, C., Boix, C., Perrouault, L., Fossey, A., Saison-Behmoaras, T., Fontecave, M., and Giovannangeli, C. (2012) Flavin Conjugates for Delivery of Peptide Nucleic Acids. *ChemBioChem* 13, 2593–2598.

(26) Rublack, N., Nguyen, H., Appel, B., Springstube, D., Strohbach, D., and Müller, S. (2011) Synthesis of Specifically Modified Oligonucleotides for Application in Structural and Functional Analysis of RNA. *J. Nucleic Acids* 2011, 1.

(27) Neises, B., and Steglich, W. (1978) Simple Method for the Esterification of Carboxylic Acids. *Angew. Chem., Int. Ed. Engl.* 17, 522–524.

(28) Torchilin, V., and Weissig, V. (2003) *Liposomes: A Practical Approach*, OUP, Oxford.

(29) Immordino, M. L., Dosio, F., and Cattel, L. (2006) Stealth liposomes: review of the basic science, rationale, and clinical applications, existing and potential. *Int. J. Nanomedicine* 1, 297–315.

(30) Kalchenko, V., Shvitiel, S., Malina, V., Lapid, K., Haramati, S., Lapidot, T., Brill, A., and Harmelin, A. (2006) Use of lipophilic near-infrared dye in whole-body optical imaging of hematopoietic cell homing. *J. Biomed. Opt.* 11, 050507.

(31) Gremse, F., Theek, B., Kunjachan, S., Lederle, W., Pardo, A., Barth, S., Lammers, T., Naumann, U., and Kiessling, F. (2014) Absorption Reconstruction Improves Biodistribution Assessment of Fluorescent Nanoparticles Using Hybrid Fluorescence-mediated Tomography. *Theranostics* 4, 960–971.

(32) Kaji, T., Kawashima, T., Sakamoto, M., Kurashige, Y., and Koizumi, F. (1991) Inhibitory effect of rhodamine B on the proliferation of human lip fibroblasts in culture. *Toxicology* 68, 11–20.

(33) Lammers, T., Hennink, W. E., and Storm, G. (2008) Tumour-targeted nanomedicines: principles and practice. *Br. J. Cancer* 99, 392–397.

(34) Ruoslahti, E., Bhatia, S. N., and Sailor, M. J. (2010) Targeting of drugs and nanoparticles to tumors. *J. Cell Biol.* 188, 759–768.

(35) McNeeley, K. M., Annapragada, A., and Bellamkonda, R. V. (2007) Decreased circulation time offsets increased efficacy of PEGylated nanocarriers targeting folate receptors of glioma. *Nanotechnology* 18, 385101.

(36) Gremse, F., Doleschel, D., Zafarnia, S., Babler, A., Jähnen-Dechent, W., Lammers, T., Lederle, W., and Kiessling, F. (2015) Hybrid  $\mu$ CT-FMT imaging and image analysis. *J. Visualized Exp.*, DOI: 10.3791/52770.

(37) Leamon, C. P., Cooper, S. R., and Hardee, G. E. (2003) Folate-liposome-mediated antisense oligodeoxynucleotide targeting to cancer cells: evaluation in vitro and in vivo. *Bioconjugate Chem.* 14, 738–747.

(38) Kirpotin, D. B., Drummond, D. C., Shao, Y., Shalaby, M. R., Hong, K., Nielsen, U. B., Marks, J. D., Benz, C. C., and Park, J. W. (2006) Antibody Targeting of Long-Circulating Lipidic Nanoparticles Does Not Increase Tumor Localization but Does Increase Internalization in Animal Models. *Cancer Res.* 66, 6732–6740.

(39) Jayapaul, J., Arns, S., Bunker, M., Weiler, M., Rutherford, S., Comba, P., and Kiessling, F. (2016) In vivo evaluation of riboflavin receptor targeted fluorescent USPIO in mice with prostate cancer xenografts. *Nano Res.* 9, 1319–1333.

(40) Rao, P. N., Crippin, J., Levine, E., Hunt, J., Baliga, S., Balart, L., Anthony, L., Mulekar, M., and Raj, M. H. G. (2006) Elevation of serum riboflavin carrier protein in hepatocellular carcinoma. *Hepatology* 35, 83–87.

(41) Arraud, N., Linares, R., Tan, S., Gounou, C., Pasquet, J.-M., Mornet, S., and Brisson, A. R. (2014) Extracellular vesicles from blood plasma: determination of their morphology, size, phenotype and concentration. *J. Thromb. Haemostasis* 12, 614–627.

(42) Gremse, F., Stärk, M., Ehling, J., Menzel, J. R., Lammers, T., and Kiessling, F. (2016) Imalytics Preclinical: Interactive Analysis of Biomedical Volume Data. *Theranostics* 6, 328–341.